Phase diagram and topological order in the modulated XYZ chain with magnetic field

Toplal Pandey and Gennady Y. Chitov
Department of Physics, Laurentian University, Sudbury, Ontario, Canada P3E 2C6

(Received 18 May 2020; revised 14 July 2020; accepted 10 August 2020; published 24 August 2020)

The XYZ antiferromagnetic spin-1/2 chain with alternation of the exchange and anisotropy couplings in the presence of uniform and staggered axial magnetic fields is studied. The analysis is done using the effective quadratic fermionic Hamiltonian resulting from the Hartee-Fock approximation. Combining the exact and the mean-field methods, the local and string order parameters on the ground-state phase diagram of the model are identified and calculated. We found a topological phase with oscillating string order with a period of four lattice spacings, not reported before for this model. A detailed analysis of patterns of the string order is given. The special XXZ limit of the model with additional U(1) symmetry brings about, in agreement with the Lieb-Schultz-Mattis theorem and its extensions, plateaux of magnetization and some additional conserving quantities. We have shown that in the XYZ chain, where the plateaux are smeared, the robust oscillating string order parameter is continuously connected to its XXZ limit. Also, the nontrivial winding number and zero-energy localized Majorana edge states, as additional attributes of topological order, are robust in that phase, even off the line of U(1) symmetry.

DOI: 10.1103/PhysRevB.102.054436

I. INTRODUCTION: MODEL AND CONTEXT

This paper is about the ground-state properties of the modulated XYZ spin-1/2 chain. Its Hamiltonian in the presence of uniform (h) and staggered (h_a) axial magnetic fields is

$$H=\sum_{n=1}^{N}\frac{J}{4}\big[(1+(-1)^n\delta)\big(\sigma_n^x\sigma_{n+1}^x+\sigma_n^y\sigma_{n+1}^y+\Delta\sigma_n^z\sigma_{n+1}^z\big)+(\gamma+(-1)^n\gamma_a)\big(\sigma_n^x\sigma_{n+1}^x-\sigma_n^y\sigma_{n+1}^y\big)\big]+\frac{1}{2}(h+(-1)^nh_a)\sigma_n^z, \tag{1}$$

where σ-s are the standard Pauli matrices. The chain has bond alternation with parameter $|\delta|\leqslant 1$. We also allowed the xy anisotropy γ to be modulated with γ_a. In this paper, we consider the antiferromagnetic ($J>0$) model at zero temperature.

The model (1) is not solvable in general, the exact solutions based on the Bethe ansatz, are available only for some special cases. For the historical references of the isotropic XXZ model with zero field, see papers by Yang and Yang [1], for more comprehensive reviews of the available exact results see, e.g., Refs. [2–4], and for a most recent account of integrability and more references, see Ref. [5]. The standard Jordan-Wigner (JW) transformation [4,6] maps (1) onto the interacting fermionic Hamiltonian

$$H=\sum_{n=1}^{N}\frac{J}{2}(1+(-1)^n\delta)\Big[(c_n^\dagger c_{n+1}+\text{H.c.})+2\Delta\Big(c_n^\dagger c_n-\frac{1}{2}\Big)\Big(c_{n+1}^\dagger c_{n+1}-\frac{1}{2}\Big)\Big]+\frac{J}{2}(\gamma+(-1)^n\gamma_a)(c_n^\dagger c_{n+1}^\dagger+\text{H.c.})+(h+(-1)^nh_a)\Big(c_n^\dagger c_n-\frac{1}{2}\Big). \tag{2}$$

Using spin-fermion dualities and mappings between the XYZ and eight-vertex models, the isotropic XXZ limit and the six-vertex model, den Nijs [7] proposed the (γ,Δ)-phase diagram of the XYZ model with zero fields and modulations. The isotropic XXZ model is gapless at $|\Delta|<1$, and its perturbations by, e.g., staggered field (h_a), dimerization (δ), or anisotropy (γ) result in a gap opening. However, the interference of different relevant perturbations can result in their cancellations at some values of model's parameters leading to gapless points or lines of quantum criticality. Scaling analysis of such perturbations and their mappings onto the operators of the eight- (six-) vertex model, lead to important conclusion about nonuniversality of the XYZ or XXZ models [7,8]. The phase diagram of the XXZ chain with uniform and staggered fields was proposed from scaling analysis in Ref. [9], see also Ref. [10]. The gapless phase of the XXZ model is the Luttinger liquid in fermionic language, and its transition into a gapped phase along the line of U(1) symmetry $\gamma=0$ is of the Berezinskii-Kosterlitz-Thouless (BKT) class [7,11].

In the context of huge recent interest in topological materials and Majorana fermions [12–15], the fermionic Hamiltonian of type (2) written more often in terms of Majorana operators, belongs to a very actively studied class of models known under the name of Kitaev-Majorana chains in recent literature. The fermionic representation (2) is the chain of interacting Majorana fermions with dimerized hopping and modulated anomalous (superconducting) pairing and chemical potential. The solvable at special symmetric points Kitaev-

Majorana models with dimerizations and spatial modulations of potential were studied very actively in recent years with the focus on their topological phases with hidden orders and Majorana edge states [16–19], similar models in more general settings were studied, e.g., in Refs. [20–22]. See Refs. [15–22] also for more references on quite vast literature on the models with Majorana fermions.

The noninteracting limit ($\Delta = 0$) of the model (2) (also known as XY chain) is known to have quite rich phase diagram [23–25]. Very recently [25] one of the gapped phases of that model was reported to possess a hidden topological order diagnosed by nonlocal string order parameter (SOP) [26], oscillating with a period of four lattice spacings. In the view of lack of information about the modulated XYZ model (1), it is natural to explore to which extend the results of Ref. [25] can be generalized for the interacting case $\Delta \neq 0$. The phase diagram of the model (1) is one of the main results of the present study.

Another more broad goal of this work aligns with the recent effort [19,25,27] to weave nonlocal (topological) orders into extended Landau paradigm. Technically, the key point is to incorporate string operators, string correlation functions, and SOPs [26] into the standard framework. The local and nonlocal order parameters are related by duality, so in a sense it is a matter of choice of variables of the Hamiltonian [19,27–31]. Another bedrock of the Landau theory is symmetry change. In the spin/fermionic systems like (1)-(2) the appearance of nonlocal SOP is accompanied by the hidden $\mathbb{Z}_2 \otimes \mathbb{Z}_2$ symmetry breaking [32]. These are internal discrete symmetries of spin reversals, and they form the Klein four-group [33], also known as the dihedral group [34], isomorphic to $\mathbb{Z}_2 \otimes \mathbb{Z}_2$ group. In some cases the duality can simply map the nonlocal order onto an average of some decoupled local operator, e.g., magnetization, and the hidden symmetry breaking becomes apparent in terms of the sublattice magnetization(s) on a dual lattice, with one or both of the Ising $\mathbb{Z}_2$ symmetries broken [19,27,30]. In general manifestations of the hidden symmetry breaking are less straightforward.

An important task addressed in this paper was to formalize the technical protocol: In the proposed unifying formalism the role of the Ginzburg-Landau effective action is played by the effective quadratic (Hartree-Fock) fermionic Hamiltonian. All local and nonlocal order parameters are calculated from the string correlation functions of Majorana fermions, evaluated from the limiting values of determinants of the block Toeplitz matrices. For the quadratic Hamiltonian, the elements of those matrices are found in a closed analytical form as functions of the effective (or renormalized) couplings of the Hamiltonian. The latter are calculated from the self-consistent minimization equations.

It appears that the notion of topological order itself is not understood uniquely in the literature. In connection to the spin chain, it appears to be associated to the additional U(1) symmetry of its isotropic XXZ limit. In such limit, the Lieb-Schultz-Mattis (LSM) theorem [6] and its subsequent generalizations [33,35,36] predict either gapless incommensurate phase without symmetry breaking, or gapped phases with broken $\mathbb{Z}_2 \otimes \mathbb{Z}_2$ symmetry, integer fillings, and plateaux of magnetization. The plateaux are sometimes viewed as a hallmark of topological order. Our understanding of topological order is not tied up to the continuous U(1) symmetry or related plateaux. The gapped phases with broken (discreet) symmetry are secured by the extension of the LSM theorem for the spin chains without continuous symmetry [37]. At $\gamma \neq 0$, the plateaux are smeared, but the robust SOP still exists and is continuously connected to its $\gamma = 0$ limit. Thus we associate topological order with a nontrivial SOP. Also, the nontrivial winding number and zero-energy localized Majorana edge states, as additional attributes of topological order, are robust in the topological phase even aside from the line of U(1) symmetry, in agreement with analogous exact results [19,25].

The rest of the paper is organized as follows. In Sec. II, we present a concise account of exact results for the noninteracting limit of the model: spectrum, phase diagram, and some average quantities. Those are building blocks to be used in the effective Hamiltonian and in the mean-field equations. Section III presents the derivation of the mean-field equations and renormalized parameters. Section IV contains the results for the XYZ chain. We present the phase diagram, local and nonlocal order parameters, winding numbers for each phase. Section V presents the results for the isotropic XXZ limit of the model. Since more analytical work can be done in this limit, more qualitative discussions of the results are presented, including the role of interaction, robustness of the mean-field approximation, and relation of the reported topological order to earlier findings of the spontaneous magnetism in this model. The algebraically ordered incommensurate gapless phase is analysed in this section as well. The results are summarized and discussed in the concluding Sec. VI.

II. NONINTERACTING LIMIT $\Delta = 0$

A. Spectrum and phase diagram

In the noninteracting limit $\Delta \equiv J_z/J = 0$, the model (1) is exactly solvable. It was first introduced and analyzed by Perk *et al.* [23]. See also Refs. [27,38–40] for related more recent work on different versions of the model. The most recent comprehensive analysis of the ground-state phase diagram of the model at $\gamma_a = 0$ and its local and nonlocal order parameters is given in Ref. [25]. It turns out that introducing alternation of anisotropy γ_a does not change the results [25] qualitatively, resulting in some minor modifications which we present below. The noninteracting results are used in the subsequent analysis of the case $\Delta \neq 0$. We will always assume $|\gamma_a| < |\gamma|$ and from now on we set $J = 1$. We also modify for further convenience the hopping term of the Hamiltonian (2) as

$$1 + (-1)^n \delta \longmapsto t + (-1)^n \delta \,. \tag{3}$$

Referring readers to Ref. [25] for technical details, in this section, we present a concise account of the results for $\gamma_a \neq 0$.

We set the lattice spacing $a = 1$ and restrict wave numbers to the reduced Brillouin zone (BZ) $k \in [-\pi/2, \pi/2]$. The band index $\alpha = 1$ and 2 serves to map the Fourier-transformed JW fermions from the 2π BZ onto the reduced zone as

$$c(k) = c_1(k) \cdot \vartheta(\pi/2 - |k|) + c_2(k - \pi) \cdot \vartheta(|k| - \pi/2)\,, \tag{4}$$

where $\vartheta(x)$ is the Heaviside step function. Then the coordinate representation of the JW fermion reads as

$$c_n = \frac{1}{\sqrt{N}} \sum_{\alpha,q} c_\alpha(q)(-1)^{(\alpha-1)n} e^{-iqn}. \tag{5}$$

The Hamiltonian (2) at $\Delta = 0$ can be written as

$$H = \frac{1}{2} \sum_k \psi_k^\dagger \mathcal{H}(k) \psi_k, \tag{6}$$

where the fermions are unified in the spinor

$$\psi_k^\dagger = (c_1^\dagger(k), c_2^\dagger(k), c_1(-k), c_2(-k)), \tag{7}$$

with the 4×4 Hamiltonian matrix

$$\mathcal{H}(k) = \begin{pmatrix} \hat{A} & \hat{B} \\ \hat{B}^\dagger & -\hat{A} \end{pmatrix}, \tag{8}$$

where

$$\hat{A} \equiv \begin{pmatrix} h + t\cos k & h_a + i\delta \sin k \\ h_a - i\delta \sin k & h - t\cos k \end{pmatrix} \tag{9}$$

and

$$\hat{B} \equiv \begin{pmatrix} -i\gamma \sin k & -\gamma_a \cos k \\ \gamma_a \cos k & i\gamma \sin k \end{pmatrix}, \tag{10}$$

The Hamiltonian has four eigenvalues [23] $\pm E_\pm$, where

$$E_\pm(k) = \sqrt{\mathfrak{C}_2(k) \pm \sqrt{\mathfrak{C}_2^2(k) - \mathfrak{C}_4(k)}}, \tag{11}$$

with

$$\mathfrak{C}_2(k) \equiv h^2 + h_a^2 + \left(t^2 + \gamma_a^2\right)\cos^2 k + (\delta^2 + \gamma^2)\sin^2 k \tag{12}$$

and

$$\mathfrak{C}_4(k) \equiv \left(h^2 - h_a^2 - \left(t^2 - \gamma_a^2\right)\cos^2 k - (\delta^2 - \gamma^2)\sin^2 k\right)^2 + (t\gamma - \delta\gamma_a)^2 \sin^2 2k \tag{13}$$

The phase diagram of the model [23] shown in Fig. 1, is found from the condition

$$\mathfrak{C}_4(k) = 0 \tag{14}$$

for the critical lines, where the model becomes gapless.

There are three phase boundaries: (i) at $\pm h_c^{(1)}$ with

$$h_c^{(1)} \equiv \sqrt{t^2 + h_a^2 - \gamma_a^2}, \ \forall \gamma, \delta, \tag{15}$$

the gap vanishes at the center of the BZ ($k = 0$).

(ii) At the edge of the BZ ($k = \pm\pi/2$), the gap vanishes on the circle

$$h^2 + \gamma^2 = h_a^2 + \delta^2, \tag{16}$$

which we will associate with the critical field $h_c^{(2)}$.

(iii) Two critical line segments at $\gamma = 0$ ($\gamma_a = 0$) correspond to the gap vanishing at the incommensurate (IC) wave vector

$$k_F = \pm \arcsin Q, \ \ Q \equiv \sqrt{\frac{t^2 + h_a^2 - h^2}{t^2 - \delta^2}}, \tag{17}$$

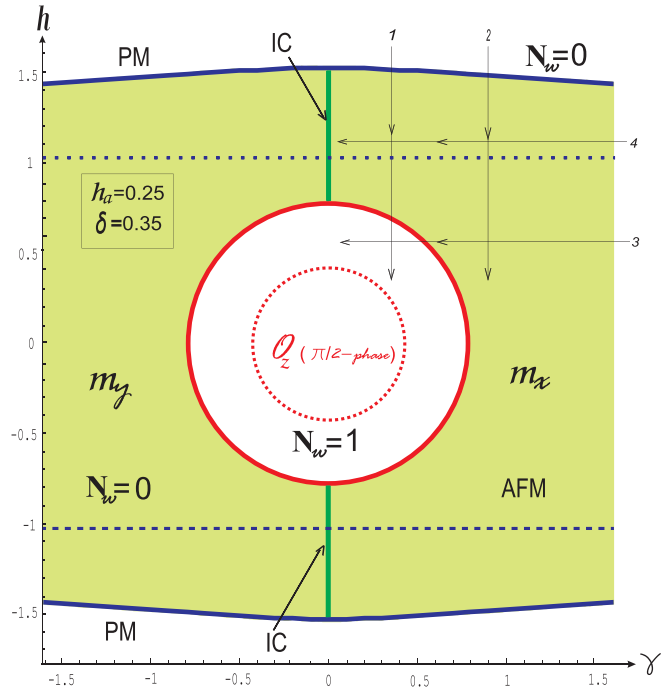

FIG. 1. Phase diagram of the model in h-γ plane ($\gamma_a = 0$). The model is critical on (i) two infinite lines $h = \pm h_c^{(1)}$ (bold blue); (ii) circle $h^2 + \gamma^2 = \mathcal{R}^2$ (bold red); and (iii) two segments $h_c^{(2)} \leqslant |h| \leqslant h_c^{(1)}$ along $\gamma = 0$ (bold green). Three phases are shown: disordered paramagnetic (PM) polarized by the axial field, planar antiferromagnetic (AFM) with local order parameters $m_{x,y}$, and topological $\mathcal{O}_z(\pi/2)$ with oscillating string order. The four paths (1–4) in parametric space are indicated by thin lines. The winding numbers N_w calculated in Sec. IV are also shown. The bold phase boundaries are calculated for interaction $\Delta = 1/2$, while their dashed counterparts correspond to noninteracting case $\Delta = 0$.

which corresponds to the Fermi momentum ($\hbar = 1$) of the JW fermions. The IC solution exists in the range of parameters $\gamma = \gamma_a = 0$, $|\delta| < 1$, and

$$\sqrt{h_a^2 + \delta^2} \leqslant |h| \leqslant \sqrt{t^2 + h_a^2}. \tag{18}$$

The Fermi momentum (17) varies continuously from $k_F = 0$ at the intersection of $\gamma = 0$ and $h = \pm\sqrt{t^2 + h_a^2}$, to $k_F = \pm\pi/2$ where the critical segments end at the intersections with the circle.

B. Spin and Majorana averages

Differentiation of the free energy with respect to h and to h_a yields two magnetizations

$$m_z = \frac{1}{N} \sum_{n=1}^{N} \langle \sigma_n^z \rangle \tag{19}$$

and

$$m_z^a = \frac{1}{N} \sum_{n=1}^{N} (-1)^n \langle \sigma_n^z \rangle, \tag{20}$$

respectively. Their explicit expressions are

$$m_z = \frac{h}{\pi}\int_0^{\pi/2}\left[\left(\frac{1}{E_+}+\frac{1}{E_-}\right) + \frac{t^2\cos^2 k + |w_a|^2}{R}\left(\frac{1}{E_+}-\frac{1}{E_-}\right)\right]dk \tag{21}$$

and

$$m_z^a = \frac{h_a}{\pi}\int_0^{\pi/2}\left[\left(\frac{1}{E_+}+\frac{1}{E_-}\right) + \frac{|w|^2+\gamma_a^2\cos^2 k}{R}\left(\frac{1}{E_+}-\frac{1}{E_-}\right)\right]dk. \tag{22}$$

We define the auxiliary parameters:

$$w \equiv h + i\gamma\sin k, \tag{23}$$

$$w_a \equiv h_a + i\delta\sin k, \tag{24}$$

$$z \equiv w w_a - t\gamma_a\cos^2 k, \tag{25}$$

$$c \equiv (ht + h_a\gamma_a)\cos k, \tag{26}$$

$$R \equiv \sqrt{c^2+|z|^2}. \tag{27}$$

The Hamiltonian (8) is diagonalized with the help of two unitary 2×2 matrices $\hat{\Phi}$ and $\hat{\Psi}$. We find

$$\hat{\Phi}(q) = \begin{pmatrix} e^{-i\theta}\beta_+ & \beta_- \\ -\beta_- & e^{i\theta}\beta_+ \end{pmatrix}, \tag{28}$$

where

$$e^{i\theta} \equiv \frac{z}{|z|} \tag{29}$$

and

$$\beta_\pm \equiv \frac{1}{\sqrt{2}}\left(1\pm\frac{c}{R}\right)^{1/2}. \tag{30}$$

The second matrix of this Bogoliubov transformation is calculated as

$$\hat{\Psi} = \hat{I}_E^{-1}\hat{\Phi}(\hat{A}-\hat{B}), \tag{31}$$

where $\hat{I}_E \equiv \mathrm{diag}(E_+, E_-)$. We introduce the Majorana fermions as

$$a_n + ib_n \equiv 2c_n^\dagger. \tag{32}$$

From the matrix

$$\hat{G}(q) \equiv \hat{\Psi}^\dagger(q)\hat{\Phi}(q), \tag{33}$$

we find the correlation function of the Majorana operators:

$$\langle ib_n a_m\rangle = \frac{1}{2\pi}\int_{-\pi}^{\pi} dq e^{-iq(m-n)}\{G_{11}(q)+(-1)^n G_{12}(q)\}, \tag{34}$$

where the matrix elements are:

$$G_{11}(q) = (t\cos q + w^*)\left\{\frac{\beta_+^2}{E_+}+\frac{\beta_-^2}{E_-}\right\} + (w_a-\gamma_a\cos q)e^{-i\theta}\beta_+\beta_-\left\{\frac{1}{E_+}-\frac{1}{E_-}\right\}, \tag{35}$$

$$G_{12}(q) = (w_a-\gamma_a\cos q)\left\{\frac{\beta_-^2}{E_+}+\frac{\beta_+^2}{E_-}\right\} + (t\cos q + w^*)e^{i\theta}\beta_+\beta_-\left\{\frac{1}{E_+}-\frac{1}{E_-}\right\}. \tag{36}$$

All the above formulas recover those of Ref. [25] in the limit $t\to 1$ and $\gamma_a\to 0$. The correlation function (34) is a building element of Toeplitz determinants [6] used to calculate local order parameters (magnetization) and nonlocal SOPs. Addition of $\gamma_a\neq 0$ only slightly numerically modifies positions of boundaries on the phase diagram and the values of correlation functions, leaving the structure of the phase diagram, the nature of its phases, and order parameters essentially the same as reported in our earlier work [25], see Fig. 1.

III. MEAN-FIELD EQUATIONS

The mean-field theory for the XYZ chain is in fact the Hartee-Fock approximation for its interacting fermionic representation (2). We use the most general decoupling [41] for the interacting term with a product of two number operators ($\hat{n}_l = c_l^\dagger c_l$) as

$$\hat{n}_l\hat{n}_m \approx \hat{n}_l\langle\hat{n}_m\rangle + \hat{n}_m\langle\hat{n}_l\rangle - \langle\hat{n}_l\rangle\langle\hat{n}_m\rangle + c_l^\dagger c_m\langle c_l c_m^\dagger\rangle + \mathrm{H.c.} + |\langle c_l c_m^\dagger\rangle|^2 + c_l^\dagger c_m^\dagger\langle c_m c_l\rangle + \mathrm{H.c.} - |\langle c_l c_m\rangle|^2. \tag{37}$$

Such approximation applied to the Heisenberg chain is known from the literature to be accurate, at least qualitatively, see, e.g., [41–44]. One cannot expect the mean-field approximation to furnish, e.g., correct critical indices to identify the universality class, but predictions of model's phase diagram and order parameters are qualitatively correct. Since $1d$ is a realm of strong fluctuations, special care needs to be exercised while dealing with the mean-field predictions for phase boundaries (critical points). They need to be cross-checked against available exact results, as we will explain below.

We introduce the following mean-field parameters:

$$\langle c_n c_{n+1}^\dagger\rangle \equiv \mathcal{K} + (-1)^n\delta\eta, \tag{38}$$

$$\langle c_n c_{n+1}\rangle \equiv P - (-1)^n\delta\eta_P, \tag{39}$$

$$\langle 1-2c_n^\dagger c_n\rangle \equiv m_z + (-1)^n m_z^a. \tag{40}$$

Using decoupling (37) and parameters (38)–(40) in (2), we obtain the approximate mean-field Hamiltonian

$$H \approx H_{MF} = N\Delta\mathcal{C} + \frac{1}{2}\sum_k \psi_k^\dagger\mathcal{H}_R(k)\psi_k\,. \tag{41}$$

The renormalized Hamiltonian $\mathcal{H}_R(k)$ is given by the same expressions as for the noninteracting case (8), (9), and (10), with the difference that the six bare couplings of the free-fermionic Hamiltonian are replaced by the remormalized parameters as follows:

$$h \longmapsto h_R \equiv h - \Delta m_z, \tag{42}$$

$$h_a \longmapsto h_{aR} \equiv h_a + \Delta m_z^a, \tag{43}$$

$$t \longmapsto t_R \equiv 1 + 2\Delta(\mathcal{K} + \delta^2\eta), \tag{44}$$

$$\delta \longmapsto \delta_R \equiv \delta(1 + 2\Delta(\mathcal{K} + \eta)), \tag{45}$$

$$\gamma \longmapsto \gamma_R \equiv \gamma - 2\Delta(P - \delta^2\eta_P), \tag{46}$$

$$\gamma_a \longmapsto \gamma_{aR} \equiv \gamma_a - 2\Delta\delta(P - \eta_P), \tag{47}$$

and the constant term is

$$\mathcal{C} = \mathcal{K}^2 - P^2 - \tfrac{1}{4}m_z^2 + \tfrac{1}{4}\left(m_z^a\right)^2 + \delta^2\left(\eta^2 - \eta_P^2 + 2\mathcal{K}\eta + 2P\eta_P\right). \tag{48}$$

Contrary to the model's bare parameters of choice, the renormalized couplings (42)–(47) are to be found from a set of six self-consistent equations obtained from minimization of the free energy. The latter is calculated from the Hartree-Fock Hamiltonian $\mathcal{H}_R(k)$. Using (38), we find equations for the bond average

$$\mathcal{K} = \frac{t_R}{2\pi}\int_0^{\pi/2} dk \cos^2 k \left\{\frac{1}{E_+} + \frac{1}{E_-} + \frac{h_R^2 + \gamma_{aR}^2\cos^2 k}{R}\left(\frac{1}{E_+} - \frac{1}{E_-}\right) + \frac{\delta_R\gamma_R\gamma_{aR}\sin^2 k}{t_R R}\left(\frac{1}{E_+} - \frac{1}{E_-}\right)\right\} \tag{49}$$

and for the dimerization susceptibility η

$$\delta\eta = \frac{\delta_R}{2\pi}\int_0^{\pi/2} dk \sin^2 k \left\{\frac{1}{E_+} + \frac{1}{E_-} + \frac{|w|^2}{R}\left(\frac{1}{E_+} - \frac{1}{E_-}\right) + \frac{t_R\gamma_R\gamma_{aR}\cos^2 k}{\delta_R R}\left(\frac{1}{E_+} - \frac{1}{E_-}\right)\right\}. \tag{50}$$

From (39), we obtain equations for the anomalous pairing amplitude

$$P = \frac{\gamma_R}{2\pi}\int_0^{\pi/2} dk \sin^2 k \left\{\frac{1}{E_+} + \frac{1}{E_-} + \frac{|w_a|^2}{R}\left(\frac{1}{E_+} - \frac{1}{E_-}\right) + \frac{t_R\delta_R\gamma_{aR}\cos^2 k}{\gamma_R R}\left(\frac{1}{E_+} - \frac{1}{E_-}\right)\right\} \tag{51}$$

and for the anomalous susceptibility

$$\delta\eta_P = -\frac{\gamma_{aR}}{2\pi}\int_0^{\pi/2} dk \cos^2 k \left\{\frac{1}{E_+} + \frac{1}{E_-} + \frac{h_{aR}^2 + t_R^2\cos^2 k}{R}\left(\frac{1}{E_+} - \frac{1}{E_-}\right) + \frac{t_R\delta_R\gamma_R\sin^2 k}{\gamma_{aR}R}\left(\frac{1}{E_+} - \frac{1}{E_-}\right)\right\}. \tag{52}$$

The uniform and staggered magnetizations (40) satisfy Eqs. (21) and (22) with their right hand sides written in terms of the renormalized couplings (42)–(47). In the following, we chose the bare coupling $\gamma_a = 0$.

The mean-field parameters (49)–(52) are fundamentally important for calculation of the phase diagram, the local and string order parameters in different phases. The representative numerical results for these parameters are shown in Fig. 2. Note that anomalous average P and η_P are not the true (superconducting) order parameters signalling spontaneous breaking of U(1) symmetry. This symmetry is intrinsically broken by model's anisotropy couplings γ, γ_a. As one can see from Fig. 2(b), in the symmetry-restoring limit γ, $\gamma_a \to 0$, the anomalous average parameters vanish.

IV. RESULTS FOR XYZ CHAIN

Before we proceed to explore predictions of the derived mean-field equations, let us first understand qualitatively possible outcomes. The way the mean-field theory is constructed, i.e., by switching to the renormalized couplings (42)–(47), makes it obvious that the interacting model has the same spectrum as in Eq. (11), but with renormalized parameters. Thus we obtain the same phases and their order parameters, conditions for the phase boundaries (gaplessness), etc., as described above for the case $\Delta = 0$ (see Ref. [25] for more details), proviso that all bare couplings are renormalized in appropriate formulas. Within present theory, no new phase with a new order parameter, other than presented on the phase diagram in Fig. 1, can occur.

Interactions, however, can bring about additional nontrivial solutions of the mean-field equations for the renormalized parameters, like, dimerization, anisotropy, uniform or staggered fields/magnetizations, even when their bare counterparts are zero. That would constitute the case of spontaneous symmetry breaking associated with a phase transition. As one can see from Fig. 2(b), the anomalous average parameters vanish in the limit $XYZ \to XXZ$. We did not find numerical signs of spontaneous breaking of the U(1) symmetry (superconductivity) at $\Delta \neq 0$. Neither we found spontaneous dimerization when bare $\delta = 0$. This is in agreement with available results for the XYZ and XXZ models [2,4,7,9]. However, it is known from exact results that $\Delta = \pm 1$ are critical points of the antiferro-/ferromagnetic phase transitions in the XXZ model [2,4]. In the XYZ chain ($\gamma \neq 0$) spontaneous antiferro-/ferromagnetism appears at $|\Delta| > 1$ [7]. To stay on the safe side and to avoid dealing with the interaction-induced magnetism in the results which follow, we will assume the regime of weak interaction $|\Delta| < 1$ in this section. The strongly interacting regime $\Delta \gtrsim 1$ is discussed in Sec. V for the XXZ chain.

The phase diagram of the model is shown in Fig. 1. Overall, the mean-field results in this regime are qualitatively similar to the noninteracting ($\Delta = 0$) case [25]. The PM-AFM boundary (15) gets modified by interactions. It is not a straight line anymore. The value for critical field $h_c^{(1)}$ is available only numerically. However, its maximum value reached in the XXZ limit is found exactly from our equations:

$$\gamma = 0: \; h_c^{(1)} = \Delta + \sqrt{1 + h_a^2}, \tag{53}$$

in agreement with earlier scaling results [9].

The topological phase with oscillating string order is located inside the circle on the phase diagram in Fig. 1.

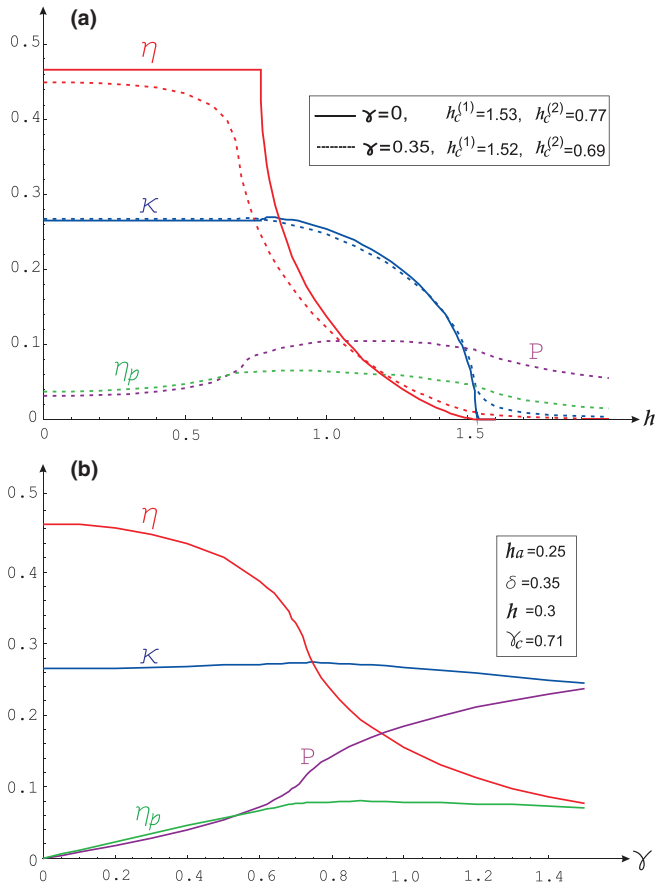

FIG. 2. Representative behavior of mean-field parameters (49)–(52) calculated for interaction $\Delta = 1/2$. (a) shows results along the path 1 on the phase diagram in Fig. 1. (b) corresponds to path 3. In addition, (a) presents results along the line $\gamma = 0$.

Quite amazingly (in the view of complexity of the six coupled mean-field equations), interactions only change the radius of the circle $\mathcal{R}$, conserving the perfect shape of this phase boundary. Numerically we found

$$\mathcal{R}(\Delta) \approx \mathcal{R}(0) + a\Delta\,, \tag{54}$$

where the radius for the noninteracting case $\mathcal{R}(0) = \sqrt{h_a^2 + \delta^2}$. The linear fit with $a \approx 0.745$, shown in Fig. 3, works quite well even at $\Delta \gtrsim 1$.

A. Induced and spontaneous magnetizations

First we present the field-induced magnetizations m_z and m_z^a as functions of the uniform magnetic field h in Fig. 4. Their explicit expressions (21) and (22) are calculated at each point with the renormalized couplings on the right hand sides, determined self-consistently from numerical solution of the mean-field equations given in the previous section.

The plots for the XYZ chain are done for two cases. The first case corresponds to the path 1 on the phase diagram in the h-γ plane shown in Fig. 1. The path crosses the PM-AFM boundary at $h = h_c^{(1)}$ and the AFM-$\mathcal{O}_z(\pi/2)$ boundary at $h = h_c^{(2)}$. The magnetizations have noticeable cusps at these critical points, which correspond to divergent susceptibilities. In case of the path 2, it crosses only the PM-AFM boundary and

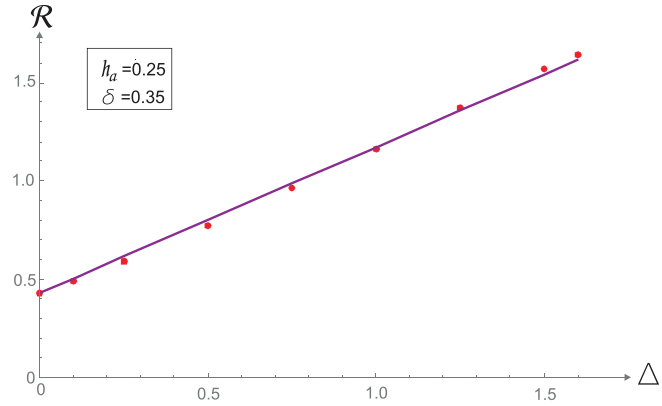

FIG. 3. Radius of the circle enclosing $\mathcal{O}_z(\pi/2)$ phase in the phase diagram Fig. 1 as a function of interaction. The linear fit with the slope $a \approx 0.745$ is shown.

bypasses the topological phase. The magnetizations demonstrate cusps at the only critical point $h_c^{(1)}$, while at $h < h_c^{(1)}$ they and their derivatives are analytical.

The phase diagram in Fig. 1 contains two conventional antiferromagnetic phases with spontaneous planar magnetizations m_x and m_y. The local order parameter m_x is calculated form the limit of the spin-correlation function which is also the correlation function of the Majorana string operators [6]:

$$\langle \sigma_L^x \sigma_R^x \rangle = \left\langle \prod_{n=L}^{R-1} [ib_n a_{n+1}] \right\rangle \underset{[R\to\infty]}{\Longrightarrow} m_x^2\,. \tag{55}$$

As we have shown in Ref. [25], this Majorana string correlation function is given by the determinant of the block Toeplitz matrix constructed from $\frac{1}{2}(R-L) \times \frac{1}{2}(R-L)$ blocks of size 2×2 with the elements given by Eq. (34). For explicit expressions of this block Toeplitz matrix we refer the reader to

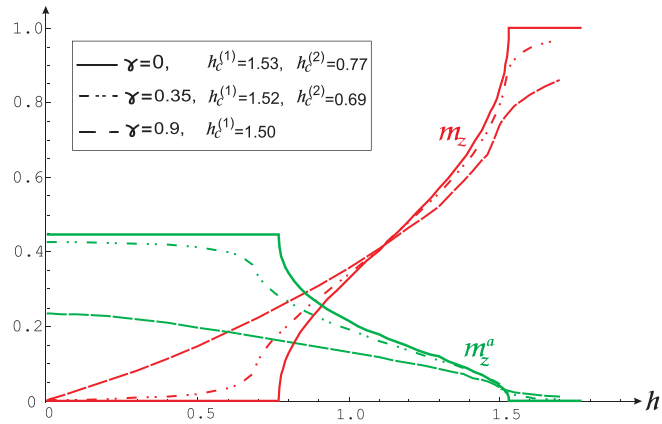

FIG. 4. Two induced magnetizations m_z (red) and m_z^a (green) vs uniform field h at $\delta = 0.35$, $h_a = 0.25$, $\Delta = 0.5$ for different γ. At $\gamma = 0$, m_z (solid line) demonstrates plateaux in the gapped phases connected by a continuous curve through the gaplees IC phase. Similar behavior is demonstrated by m_z^a. Dashed-dotted lines correspond to path 1 shown in the phase diagram Fig. 1. Dashed lines correspond to path 2. The magnetizations show noticeable cusps at the critical fields $h_c^{(1)}$ (path 2); $h_c^{(1)}$ and $h_c^{(2)}$ (paths $\gamma = 0$ and 1), when the paths cross phase boundaries.

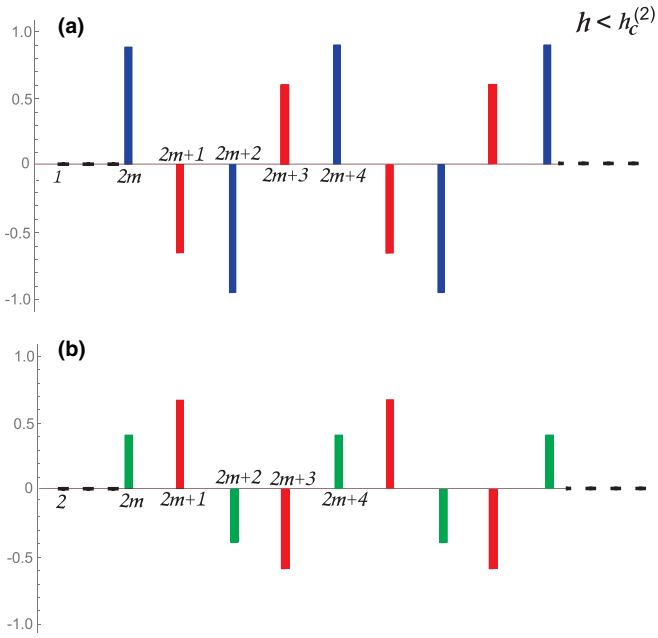

FIG. 5. Visualization of the oscillating string order inside the circle at the point $h = 0.2$ on path 1 (Fig. 1) for $h_a = 0.25$, $\delta = 0.35$, $\gamma = 0.35$, and $\Delta = 1/2$. (a) shows $\mathfrak{D}_{zz}(1, N)$ (58) with alternating limiting values $\pm\mathcal{O}_{z,1}^2$ (blue) and $\pm\mathcal{O}_{z,3}^2$ (red). (b) shows $\mathfrak{D}_{zz}(2, N)$ with similar parameters $\pm\mathcal{O}_{z,2}^2$ (green) and $\pm\mathcal{O}_{z,3}^2$.

Ref. [25]. At each point in the parametric space, the elements (34) of this matrix are calculated with renormalized couplings determined from the mean-field equations. The results for spontaneous magnetization are given in Fig. 6. The numerical values of the parameters we present in that figure are stable in the fourth decimal place for the $M \times M$ matrices of sizes $M \gtrsim 30$. In immediate vicinities of the critical points the order parameters are checked to decay smoothly as $M \to \infty$. The expressions for m_y are obtained along the same lines. Numerical values satisfy useful relation $m_y(-\gamma) = m_x(\gamma)$, verified explicitly.

B. Nonlocal string order

Now we address the topological phase with nonlocal string order inside the circle in Fig. 1, first reported in Ref. [25] for noninteracting case. It turns out that the fermionic interaction renormalizes the phase boundary and SOPs, but does not alter the nature of the order in this phase. To quantify this type of order, we use the string operator

$$O_z(n) \equiv \prod_{l=1}^{n} \sigma_l^z = \prod_{l=1}^{n} [ib_l a_l] \tag{56}$$

and related string correlation function

$$\mathfrak{D}_{zz}(L, R) \equiv \langle O_z(L-1) O_z(R) \rangle = \left\langle \prod_{l=L}^{R} [ib_l a_l] \right\rangle. \tag{57}$$

Following the original proposal by den Nijs and Rommelse [26], the SOP was defined and detected in the subsequent work on the spin chains, see, e.g., Refs. [32,45,46]. The SOP was defined (up to some minor variations) as the limit of the string-string correlation function, which is not convenient, since such SOP has a wrong dimension of square of the order parameter. The definition we use, due to Berg *et al.* [47], is more consistent with the standard theory of critical phenomena, and the critical index of the (string) order parameter β correctly enters all the hyperscaling relations [27]. The correlation function (57) is calculated from the determinant of the block Toeplitz matrices, built from elements (34). These matrices are given explicitly in Ref. [25].

Inside the circle, $\mathfrak{D}_{zz}$ oscillates with the period of four lattice spacings (i.e., *twice the unit cell*), see Fig. 5. Doubling of the translational period by the string order is a sign of spontaneous breaking of the hidden $\mathbb{Z}_2 \otimes \mathbb{Z}_2$ symmetry. This phase is labeled as $\mathcal{O}_z(\pi/2)$ to distinguish it from the plain behavior of $\mathfrak{D}_{zz}$ in the PM phase. Since $\mathfrak{D}_{zz}(L, R) \neq \mathfrak{D}_{zz}(R - L)$, we need three parameters to account for the string order:

$$\mathfrak{D}_{zz}(L, R) \xrightarrow[R\to\infty]{} \begin{cases} (-1)^m \mathcal{O}_{z,1}^2, & L = 1,\ R = 2m \\ (-1)^m \mathcal{O}_{z,2}^2, & L = 2,\ R = 2m \\ (-1)^{m+L} \mathcal{O}_{z,3}^2, & L = 1,\ R = 2m+1 \text{ or } L = 2,\ R = 2m+1 \end{cases}. \tag{58}$$

The ordering patterns (58) detected from nondecaying oscillations of the string correlation function for a particular parametric point in the $\mathcal{O}_z(\pi/2)$ phase, are depicted in Fig. 5. The magnitudes of the SOPs $\mathcal{O}_{z,i}$ along different paths on the phase diagram Fig. 1 are given in Figs. 6(a) and 6(c). At each point the SOP is calculated with the remormalized couplings determined from numerical solution of the self-consistent mean-field equations. Similarly to the noninteracting case [25], the other two components of the SOP $\mathcal{O}_x$ and $\mathcal{O}_y$ vanish when $h \neq 0$ and $h_a \neq 0$.

The string correlation function $\mathfrak{D}_{zz}$ in the PM saturated phase is always positive and essentially monotonous. For completeness we plot in Fig. 6 the PM SOP defined as $\lim_{R\to\infty} \mathfrak{D}_{zz}(L, R) = \mathcal{O}_z^2$.

There are interesting limiting cases of the topological string order. Two alternating (bare) parameters of the model, h_a and δ generate the topological phase, see Fig. 1. The radius of its boundary $\mathcal{R} = \sqrt{h_{aR}^2 + \delta_R^2}$. We check from the mean-field equations that at $|\Delta| < 1$, $h_{aR} \propto h_a$ and $\delta_R \propto \delta$, i.e., turning off one of those parameters, turns off its renormalized counterpart as well. Although the four lattice spacing periodicity of the string correlation function (58) is preserved, its ordering patterns are distinct. There are often physically interesting situations when there is an alternating component

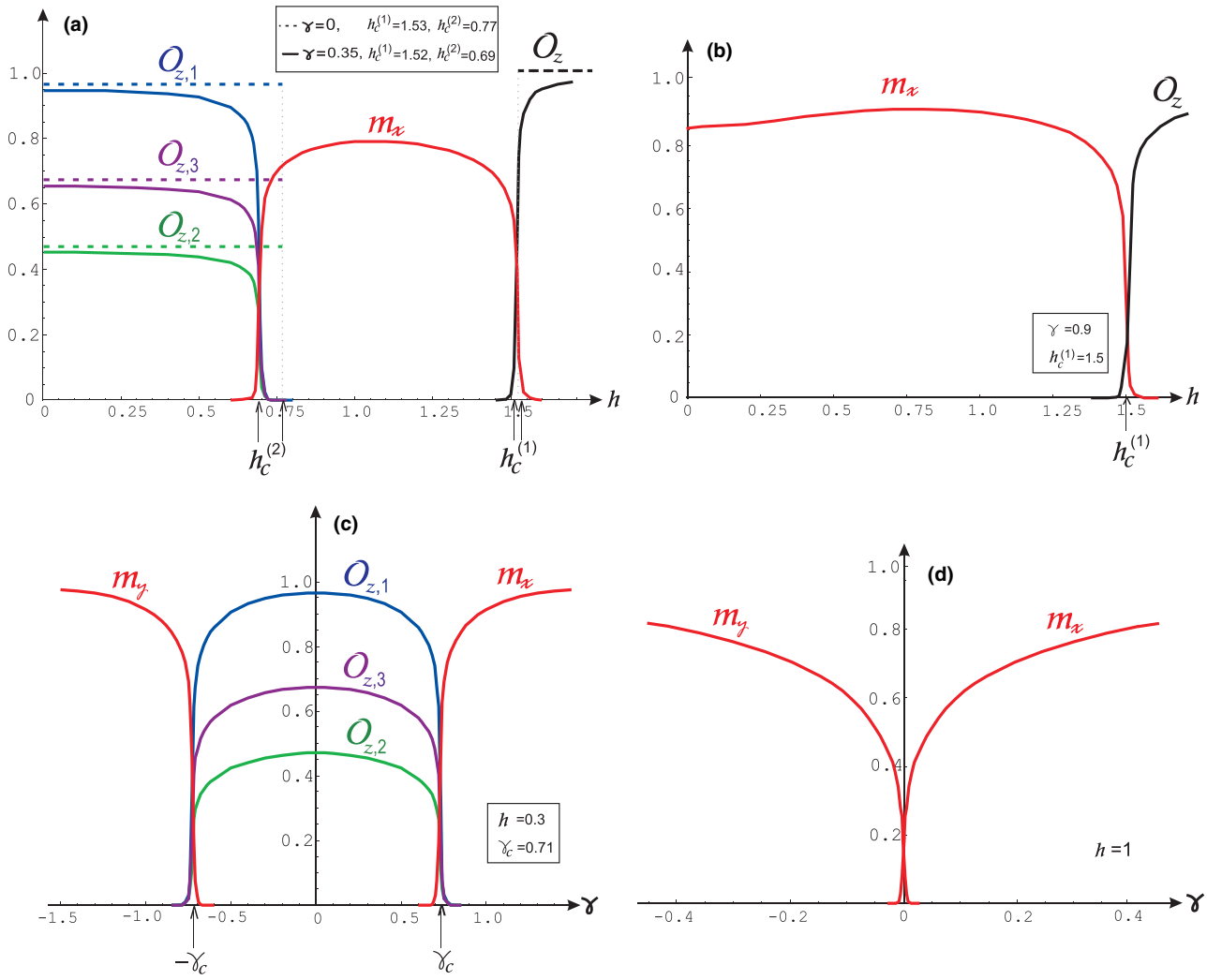

FIG. 6. Spontaneous planar magnetizations $m_{x,y}$ and modulated string order parameters $\mathcal{O}_{z,i}$ numerically calculated from the $2N \times 2N$ matrices with $N = 70$. The panels (a-d) correspond to the paths 1-4 on the phase diagram shown in Fig. 1 ($h_a = 0.25$ and $\delta = 0.35$). In the AFM phases, $m_{x,y} \neq 0$ and $\mathcal{O}_{z,i} = 0$. In the PM phase $h > h_c^{(1)}$, $\mathcal{O}_z \neq 0$ and plainly monotonous. The exact values of the critical parameters $h_c^{(1)}$, $h_c^{(2)}$, γ_c (shown by arrows) are calculated from renormalized Eqs. (15) and (16). Nonvanishing small tails of the order parameters seen in the immediate vicinities of the critical points are the finite-size effects, checked to die off as $N \to \infty$. The special case $\gamma = 0$ when all SOPs become step-like functions is shown in (a).

of the magnetic field (or modulated chemical potential, when dealing with various versions of the Kitaev-Majorana models (2), while the dimerization is absent. Or vice versa, quite often one is dealing with dimerized models with uniform magnetic field (chemical potential). We find for the former case,

$$h_a = 0,\ \delta \neq 0: \quad \mathcal{O}_{z,1} \neq 0, \quad \mathcal{O}_{z,2} = \mathcal{O}_{z,3} = 0, \tag{59}$$

and for the latter,

$$h_a \neq 0, \quad \delta = 0: \ \mathcal{O}_{z,1} = \mathcal{O}_{z,2} = \mathcal{O}_{z,3}, \tag{60}$$

These properties hold for the noninteracting case ($\Delta = 0$) as well as in the presence of interactions ($\Delta \neq 0$). Two cases of the ordering patterns are shown in Fig. 7.

With the help of duality mappings [27] and identities for the string operators [25], we find the SOP analytically for $\Delta = 0$ inside the circle for the case $h_a = 0$ along the line $h = 0$:

$$h_a = h = 0: \ \mathcal{O}_{z,1}^2 = 2\left[\frac{(\delta^2 - \gamma^2)}{((1 \pm \delta)^2 - \gamma^2)^2}\right]^{1/4}. \tag{61}$$

The above result yields the critical index of the order parameter $\beta = 1/8$ in the universality class of the 2D Ising model. Equation (61) is derived for $\Delta = 0$, the interacting result within the present approximation is obtained by promoting bare couplings in (61) to the renormalized ones.[1]

Note that the case (59) applies for the dimerized isotropic ($\gamma = 0$) Heisenberg chain without magnetic field. In the SU(2) limit $\Delta = 1$, the noninteracting result (61) can be improved. The magnitude of the SOP $\mathcal{O}_{z,1}$ was calculated by

[1]It should be kept in mind that the critical indices found for $\Delta = 0$ are not valid for the interacting case [7,8].

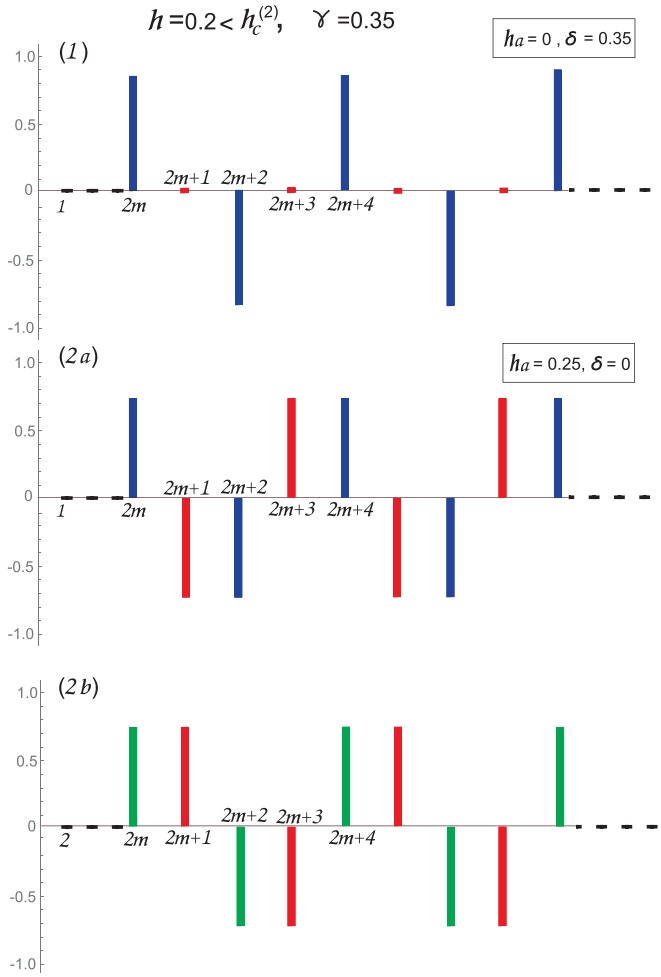

FIG. 7. Visualization of the oscillating string order inside the circle at the point $h = 0.2$ on path 1 (Fig. 1) with $\gamma = 0.35$ and $\Delta = 1/2$ for two special cases. (1) For $h_a = 0$ and $\delta = 0.35$, the string order shown in Fig. 5(b) vanishes, since $\mathcal{O}_{z,2} = \mathcal{O}_{z,3} = 0$, while the order shown in Fig. 5(a) reduces to the pattern (1) above. (2) For $h_a = 0.25$ and $\delta = 0$, $\mathcal{O}_{z,2} = \mathcal{O}_{z,2} = \mathcal{O}_{z,3} \neq 0$, and the patterns shown in Fig. 5 become the same, up to a singe lattice spacing translation, as shown in (2a) and (2b) above.

Hida via bosonization [45], however the oscillating pattern of the string order shown in Fig. 7(1) was not reported before.

To deal with the string order in a more unified and compact way, we introduce a new function

$$\mathfrak{D}^{(+)}_{zz}(n) \equiv \mathfrak{D}_{zz}(1,n) + \mathfrak{D}_{zz}(2,n) \tag{62}$$

From visual inspection of the patterns shown in Figs. 5(a) and 5(b) one can easily check that $\mathfrak{D}^{(+)}_{zz}(n)$ has its ordering pattern similar to the one shown in Fig. 7(1), i.e.,

$$\mathfrak{D}^{(+)}_{zz}(n) \xrightarrow[n\to\infty]{} \cos\left(\frac{\pi}{2}n\right)\mathcal{O}^2_{z,+}\,, \tag{63}$$

where

$$\mathcal{O}^2_{z,+} \equiv \mathcal{O}^2_{z,1} + \mathcal{O}^2_{z,2}\,. \tag{64}$$

From inspection of Fig. 7 one can check as well that the special cases (59) and (60) can be united under the same pattern of Eq. (63).

C. Winding number

For each phase we also find the winding number. The calculation outlined in Ref. [25], for the quadratic Hamiltonian (8)–(10) leads to the following result:

$$N_w = \frac{1}{2\pi i}[\ln\lambda_+(k) + \ln\lambda_-(k))]^{\frac{\pi}{2}-}_{-\frac{\pi}{2}+}\,, \tag{65}$$

where

$$\lambda_\pm(k) = h \pm \big(h_a^2 + (t^2 - \gamma_a^2)\cos^2 k + (\delta^2 - \gamma^2)\sin^2 k - i(t\gamma - \delta\gamma_a)\sin 2k\big)^{1/2} \tag{66}$$

are the eigenvalues of $\hat{D}(k) \equiv \hat{A}(k) + \hat{B}(k)$. One can establish an important relation between parameter $\mathfrak{C}_4$ of the Hamiltonian's spectrum, defined by (13), and eigenvalues (66):

$$\mathfrak{C}_4 = |\lambda_+|^2|\lambda_-|^2\,. \tag{67}$$

A simple comparison of the condition (14) for quantum criticality and Eq. (67) leads to the following conclusion: *topological winding number (mod 2) can change only upon crossing gapless phase boundary*. Within the present approach, numbers N_w in different phases of interacting model are calculated using Eqs. (65) and (66) with renormalized couplings. Their values are shown in Fig. 1. Only the phase with oscillating string order is topologically nontrivial, $N_w = 1$.

V. ISOTROPIC CHAIN

In this section, we present the results for isotropic XXZ chain, that is the limit $\gamma = \gamma_a = 0$. It turns out that a considerable progress can be achieved in analytical treatments, making the outcome more transparent for intuitive grasp.

A. Noninteracting XX limit ($\Delta = 0$)

Most of the formulas of Sec. II for free fermions can be brought to a closed form of standard mathematical functions. The content of this subsection is implicitly present in the earlier work [25], but the XX limit was not specifically analyzed in that paper. The spectrum (11) becomes

$$E_\pm(k) = h \pm \xi,\;\; \xi \equiv \sqrt{h_a^2 + t^2\cos^2 k + \delta^2\sin^2 k}\,. \tag{68}$$

To better understand results of this section, it is convenient to write the ground-state energy per site

$$f = -\frac{1}{2\pi}\int_0^{\pi/2}(|E_+| + |E_-|)dk \tag{69}$$

as

$$f = \frac{1}{2\pi}\int_{-\pi/2}^{\pi/2}\varepsilon_{\rm eff}(k)dk. \tag{70}$$

The effective spectrum $\varepsilon_{\rm eff}(k)$ is shown in Fig. 8 for three phases. From (68) and (69), we find the h-independent effective spectrum $\varepsilon_{\rm eff}(k) = -\xi$ in the topological phase ($h < h_c^{(2)}$). In the IC gapless phase ($h_c^{(2)} < h < h_c^{(1)}$), the parabolic spectrum $\varepsilon_{\rm eff}(k) = -\xi$ at $|k| < k_F$ with the Fermi momentum given by Eq. (17), becomes a flat band $\varepsilon_{\rm eff}(k) = -h$ at $k_F < |k| < \pi/2$. The Fermi sea shrinks with the growth of the field, as shown in Fig. 8, and in the PM phase ($h > h_c^{(1)}$) the whole band is flat, $\varepsilon_{\rm eff}(k) = -h$.

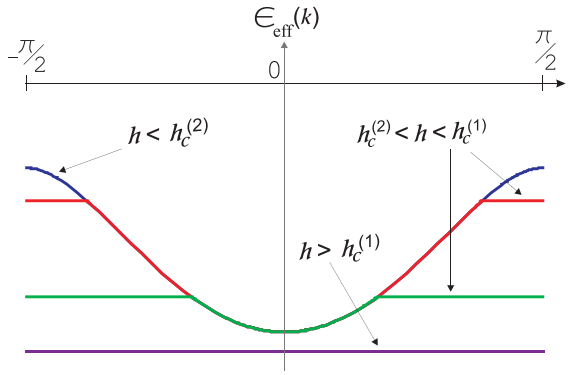

FIG. 8. The effective single-particle spectrum $\varepsilon_{\text{eff}}(k)$ in three phases at different values of the uniform field.

Analytically, we find

$$f = \begin{cases} -\frac{1}{2}h, & h > h_c^{(1)} \\ -\frac{1}{\pi}\sqrt{t^2+h_a^2}\mathbf{E}(k_F,\kappa^2)- & \\ -\frac{1}{2}h\left(1-\frac{2}{\pi}k_F\right), & h \in \left[h_c^{(2)}, h_c^{(1)}\right] \\ -\frac{1}{\pi}\sqrt{t^2+h_a^2}\mathbf{E}(\kappa^2), & h < h_c^{(2)} \end{cases}. \tag{71}$$

Here, $\mathbf{E}$ is the elliptic integral of the second kind, and

$$\kappa^2 \equiv \frac{t^2-\delta^2}{t^2+h_a^2}. \tag{72}$$

The uniform magnetization derived from Eq. (21)

$$m_z = \frac{1}{2} + \frac{1}{\pi}\int_0^{\pi/2} \text{sign}(E_-)dk \tag{73}$$

or obtained directly from differentiation of (71), demonstrates two plateaux in the gapped phases, connected by a continuous curve in between:

$$m_z = \begin{cases} 1, & h > h_c^{(1)} \\ 1-\frac{2}{\pi}k_F, & h \in \left[h_c^{(2)}, h_c^{(1)}\right] \\ 0, & h < h_c^{(2)} \end{cases}. \tag{74}$$

The above results is in agreement with the arguments of Ref. [35], generalizing the Lieb-Schultz-Mattis (LSM) theorem [6] for nonzero field. According to another formulation of the LSM theorem in terms of fermions [36] [cf. Eq. (40)], the plateaux of magnetization correspond to integer fermionic fillings per unit cell, and the filling can admit noninteger values only in the gapless phase, leading to a smooth evolution of $m_z \in [0, 1]$ at $h \in [h_c^{(2)}, h_c^{(1)}]$.

To unify and generalize the analysis of phases done in Sec. II and to directly relate it to the LSM theorem [6,36], we analytically continue the spectrum of the model onto the complex plane $z \in \mathbb{C}$ with $z = e^{ik}$ [4]. In the isotropic limit, the eigenvalues $\lambda_\pm$ defined by Eq. (66) become the eigenvalues of the Hamiltonian (68), so the condition of the quantum criticality (14) with Eq. (67) reads

$$|E_+(z)|^2|E_-(z)|^2 = 0\,. \tag{75}$$

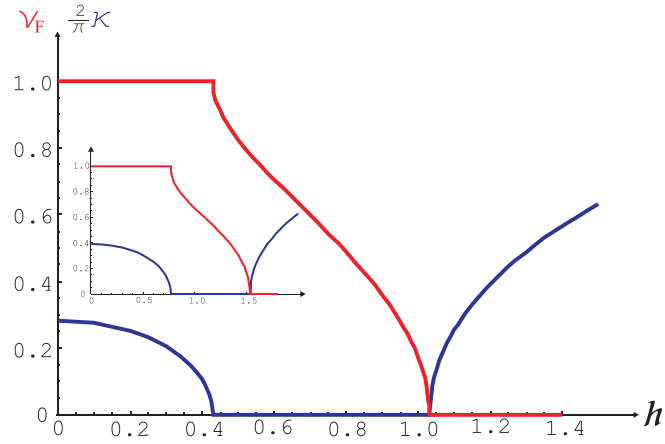

FIG. 9. Real and imaginary parts of the complex wave vector k_+ giving the values of the fermionic filling per unit cell $\nu_F = 2/\pi k_F$ and inverse correlation length $\xi^{-1} \propto \kappa$ for the three phases. The main plot is done for noninteracting model with $h_a = 0.25$ and $\delta = 0.35$. The inset shows the same parameters for the interacting case with $\Delta = 0.5$.

Using Q defined in Eq. (17) and extended to $Q \in \mathbb{C}$, we find two roots of (75)

$$z_\pm = e^{ik_\pm} = \Lambda_\pm, \text{ with } \Lambda_\pm \equiv iQ \pm \sqrt{1-Q^2}\,, \tag{76}$$

The roots $\Lambda_\pm$ encode important information about three phases. (1) In the IC phase $Q \in \mathbb{R}$ and $0 < Q < 1$. The roots are complex conjugate $\Lambda_+ = \Lambda_-^*$ and $|\Lambda_\pm| = 1$. The wave vectors $k_\pm \in \mathbb{R}$ and we can pick $k_+ = k_F$ corresponding to the known solution (17). The real wave vector k_F defines the period of oscillations of correlation functions [see Eq. (95) below] and controls the (IC) filling (Fermi level) of the parabolic band $\nu_F = 2/\pi k_F$, see Figs. 8 and 9.

(2) In the PM phase $Q = i|Q|$ is imaginary, and it leads to the imaginary $k_\pm = -i \ln \Lambda_\pm$, see Fig. 9:

$$k_F = \text{Re}k_\pm = 0, \tag{77}$$

$$\kappa = \text{Im}k_+ = -\ln(\sqrt{1+|Q|^2} - |Q|). \tag{78}$$

The nonvanishing imaginary part of the complex root k_+ gives the inverse correlation length [4], and it is responsible for the exponential decay of correlation functions in gapped phases. In the vicinity of the PM transition $h \to h_c^{(1)} + 0$: $|Q| \ll 1$, and $\kappa \approx |Q| \propto (h - h_c^{(1)})^{1/2}$. The vanishing real part of the root $k_F = 0$ means monotonous behavior of correlation functions without oscillations.

Note that probing the correlation length in the limit $\gamma \to 0$ is subtle in the PM (polarized) phase. In this case, $m_z = \mathcal{O}_z = 1$ and $m_x = m_y = 0$. Moreover, the correlation functions are featureless, i.e., $\langle \sigma_L^z \sigma_R^z \rangle = 1$ and $\langle \sigma_L^x \sigma_R^x \rangle = \langle \sigma_L^y \sigma_R^y \rangle = 0, \forall L, R$. (These functions were first found by Barouch and McCoy in [48] for the case $h_a = \delta = 0$). The string correlation functions are found to behave in a similar way, i.e., $\mathcal{D}_{zz} = 1$ and $\mathcal{D}_{xx} = \mathcal{D}_{yy} = 0$ at $\gamma = 0$. As one can find in Table 1.2 of the book by Franchini [4] at $h > 1$ and $\gamma \neq 0$ ($h_a = \delta = 0$), the spin correlation function

$$\langle \sigma_1^x \sigma_n^x \rangle \simeq X_D \frac{\Lambda_+^{-n}}{\sqrt{n}} \text{ at } n \gg 1,$$

where Λ_+ defined as in Eq. (76), determines the correlation length and agrees with the $\gamma \to 0$ result (78). Vanishing of the correlation function in the above equation is due to prefactor $X_D \to 0$ as $\gamma \to 0$ [4]. No analytical results are available for the spin or string correlation functions in the general case $h_a \neq 0$ and $\delta \neq 0$, but we infer from numerical calculations that those functions have: (i) rapid decrease with n; (ii) vanishing amplitudes; (iii) finite gap and thus meaningful definition of the correlation length in the limit $\gamma \to 0$, similar to the equation above. Another way to probe the finite gap (inverse correlation length) at $\gamma = 0$, is to consider nonzero temperature, when one expects temperature corrections to the correlation and/or response functions $\propto \exp(-\mathcal{O}(1)\kappa/T)$.

(3) For the $\mathcal{O}_z(\pi/2)$ phase, it is convenient to use $V \equiv \sqrt{1-Q^2}$. In this phase $V = i|V|$ is imaginary, leading to

$$k_F = \mathrm{Re}k_+ = \frac{\pi}{2}, \tag{79}$$

$$\kappa = -\mathrm{Im}k_+ = \ln(\sqrt{1+|V|^2}+|V|). \tag{80}$$

The real part of the root $k_F = \pi/2$ corresponds to the constant filling $\nu_F = 1$ in this phase and $\pi/2$ oscillations of the string correlation function (63). Near transition point $h \to h_c^{(2)} - 0$: $|V| \ll 1$ and $\kappa \approx |V| \propto (h_c^{(2)} - h)^{1/2}$, in agreement with the expected gap closing.

The above results for real and imaginary parts of the complex roots $k_\pm$ are depicted in Fig. 9. In agreement with general arguments [36] and with Fig. 9, the magnetization in all three phases can be related to the filling as $m_z = 1 - \nu_F$.

Qualitatively, the integer-valued fermionic fillings connected by a continuous curve through the gapless phase of Fig. 9, are due to the flat piece of the effective spectrum shown in Fig. 8. An interesting topological transition known as fermionic condensation [49] is signalled by appearance of a continuous real filling smoothly connecting between two integer values (1,0) of the step function predicted by the Landau Fermi-liquid theory. One needs a flat band piece of the single-particle spectrum for such noninteger filling to occur. The flat band and fermionic condensation [50] can model linear-T resistivity in the so-called Planckian metal [51,52]. These analogies are worth exploring further.

Two complex roots $\Lambda_\pm$ are also the eigenvalues of the transfer matrix which generates the wave function of the zero-energy edge Majorana fermion [19]. Our findings predict that the localized Majorana edge state in the $\mathcal{O}_z(\pi/2)$ phase has the wave function with the inverse penetration depth $\propto \kappa$. The exponential decay of the wave function into the bulk is modulated by $\pi/2$ oscillations. In the IC phase the edge state gets delocalized, since $\kappa = 0$.

The staggered magnetization found from Eq. (22) as

$$m_z^a = \frac{h_a}{\pi}\int_0^{\pi/2}\frac{dk}{\xi}(1-\mathrm{sign}(E_-)) \tag{81}$$

leads to

$$m_z^a = \begin{cases} 0, & h > h_c^{(1)} \\ \frac{2h_a}{\pi\sqrt{t^2+h_a^2}}\mathbf{F}(k_F,\kappa^2), & h \in \left[h_c^{(2)}, h_c^{(1)}\right] \\ \frac{2h_a}{\pi\sqrt{t^2+h_a^2}}\mathbf{K}(\kappa^2), & h < h_c^{(2)} \end{cases}. \tag{82}$$

Here, $\mathbf{K}$ and $\mathbf{F}$ are, respectively, the complete and incomplete elliptic integrals of the first kind.

The bond average and dimerization susceptibility (38) can be also found in a closed form via elliptical functions [53]. Indeed,

$$\mathcal{K} = \frac{1}{2\pi}\int_0^{\pi/2} dk\frac{\cos^2 k}{\xi}(1-\mathrm{sign}(E_-)) \tag{83}$$

yields

$$\mathcal{K} = \begin{cases} 0, & h > h_c^{(1)} \\ \frac{\sqrt{t^2+h_a^2}}{\pi(t^2-\delta^2)}[\mathbf{E}(k_F,\kappa^2) - (1-\kappa^2)\mathbf{F}(k_F,\kappa^2)], & h \in \left[h_c^{(2)}, h_c^{(1)}\right] \\ \frac{\sqrt{t^2+h_a^2}}{\pi(t^2-\delta^2)}[\mathbf{E}(\kappa^2) - (1-\kappa^2)\mathbf{K}(\kappa^2)], & h < h_c^{(2)} \end{cases}. \tag{84}$$

The dimerization susceptibility

$$\eta = \frac{1}{2\pi}\int_0^{\pi/2} dk\frac{\sin^2 k}{\xi}(1-\mathrm{sign}(E_-)) \tag{85}$$

is found as

$$\eta = \begin{cases} 0, & h > h_c^{(1)} \\ \frac{\sqrt{t^2+h_a^2}}{\pi(t^2-\delta^2)}[\mathbf{F}(k_F,\kappa^2) - \mathbf{E}(k_F,\kappa^2)], & h \in \left[h_c^{(2)}, h_c^{(1)}\right] \\ \frac{\sqrt{t^2+h_a^2}}{\pi(t^2-\delta^2)}[\mathbf{K}(\kappa^2) - \mathbf{E}(\kappa^2)], & h < h_c^{(2)} \end{cases}. \tag{86}$$

In the isotropic limit, two anomalous parameters (39) breaking the particle number conservation, $P = \eta_P = 0$ due to U(1) symmetry.

Some additional progress in analytical evaluation of the string correlation function (57) can be made for XX chain. The Majorana correlation function (34) gets simplified. Introducing

$$G^\pm(k) \equiv G_{11}(k) \pm G_{12}(k) \tag{87}$$

and

$$g^\pm \equiv (t\cos k \pm h_a \pm i\delta\sin k)/\xi\,, \tag{88}$$

we find

$$G^\pm(k) = \tfrac{1}{2}(1+\mathrm{sign}(E_-)) + \tfrac{1}{2}(1-\mathrm{sign}(E_-))g^\pm. \tag{89}$$

The above equation yields for the gapped phases

$$G^\pm(k) = \begin{cases} 1, & h > h_c^{(1)} \\ g^\pm, & h < h_c^{(2)} \end{cases} \tag{90}$$

and for the gapless IC phase at $h_c^{(2)} < h < h_c^{(1)}$,

$$G^{\pm}(k) = \begin{cases} 1, & k > k_F \\ g^{\pm}, & k < k_F \end{cases}. \tag{91}$$

At $h > h_c^{(1)}$, the block Toeplitz matrix for evaluation of $\mathfrak{D}_{zz}$ (cf. Ref. [25] its explicit form) becomes just a unit matrix for any choice of L and R in (57). So we find the exact result for the SOP:

$$\mathcal{O}_z = 1, \quad h > h_c^{(1)}. \tag{92}$$

The above result for the average of strings of σ^z operators (56) is in sync with the existence of plateau of magnetization $m_z = \langle \sigma^z \rangle = 1$.

At $h < h_c^{(2)}$, the SOPs $\mathcal{O}_{z,i}$ form step-like parabolic lines along h, similar to Eqs. (82), (84), and (86) [54]. The values of $\mathcal{O}_{z,i}$ are available via numerical calculations only. However, in case $h_a = 0$ the result (61) can be used to find SOP inside the circle along the line $\gamma = 0$:

$$h_a = \gamma = 0, \ |h| < h_c^{(2)} : \ \mathcal{O}_{z,1}^2 = 2\frac{\delta^{1/2}}{1+\delta}. \tag{93}$$

The model at $\gamma = 0$ with additional U(1) symmetry belongs to a separate universality class with the central charge $c = 1$ [4]. From (93) we infer the index of the order parameter $\beta = 1/4$ in the vicinity of the critical point $\delta = 0$.[1] Unfortunately, no progress is made at this point in analytical evaluation of SOPs beyond two special cases (61) and (93).

Two plateaux of m_z have a certain analogy with quantized Hall conductance, proportional to the topological Chern number [55]. In the isotropic limit the eigenvalues $\lambda_\pm$ defined by Eq. (66) become the eigenvalues of the Hamiltonian (68). In such a case, the winding number (65) and magnetization (73) are simply related in the gapped phases:

$$m_z = 1 - N_w \tag{94}$$

The IC gapless phase does not have long-range string order, since all three $\mathcal{O}_{z,i} = 0$ on the right hand side of (58). [In the limit $\gamma \to 0$, parameters $\mathcal{O}_{z,i}$ vanish abruptly as $h \to h_c^{(2)} + 0$ and $h \to h_c^{(1)} - 0$, see Fig. 6(a) for visualization]. However the gapless phase is *algebraically ordered*, demonstrating power-law decaying string-string correlation function with the IC oscillations:

$$\mathfrak{D}_{zz}(1,n) = \frac{\mathcal{A}}{\sqrt{n}} \cos(k_F n). \tag{95}$$

In the above formula the coefficient $\mathcal{A}$ is nonuniversal, while the critical index of the correlation function $\eta = 1/2$. The latter along with other two indices $\nu = 1$ and $\beta = 1/4$ satisfy all scaling relations. We found a perfect agreement between Eq. (95) and direct numerical calculation of the string correlation function. For a particular choice of parameters yielding $k_F = \pi/6$, the results are shown in Fig. 10(a) with $\mathcal{A} = 1/\pi^{1/8} \approx 0.87$.

B. Interacting XXZ limit ($\Delta \neq 0$)

1. Plateaux, parabolic lines, string order, and oscillations

To deal with the regime of weak interactions $\Delta \lesssim 1$, we need to replace the bare parameters in the equations of the previous subsection by the renormalized quantities. Having almost all results expressed via standard functions does not rescind the task of extensive numerical calculations, since critical fields $h_c^{(1,2)}$ and remormalized couplings must be found from self-consistent mean-field equations for each point in the four-dimensional space of bare parameters. (Two parameters are eliminated from our analysis, since we found $\gamma_R = \gamma_{aR} = 0$ in the isotropic limit).

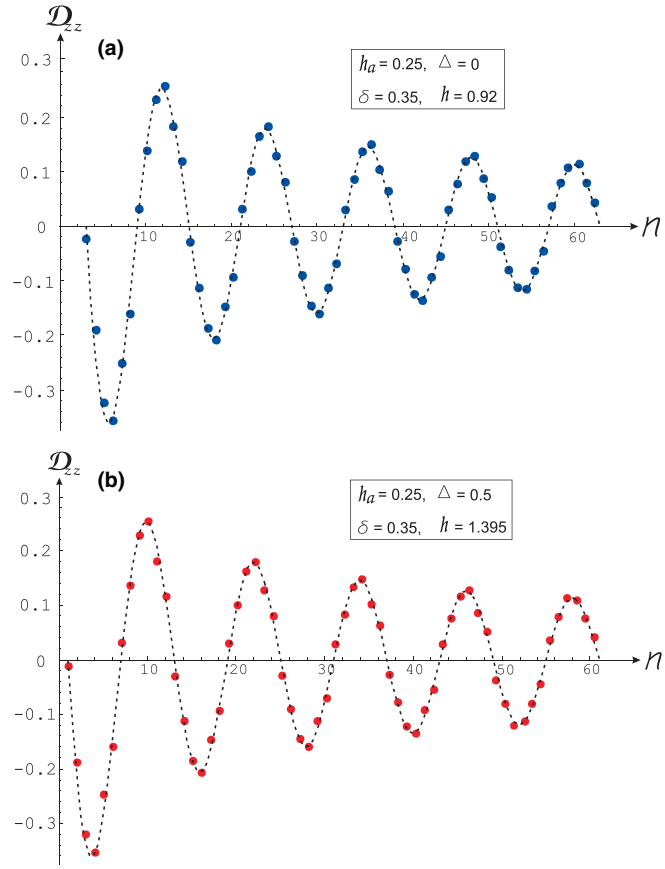

FIG. 10. Power-law decaying oscillations of the string correlation function $\mathfrak{D}_{zz}(1,n)$ in the gapless IC phase. (a) shows direct numerical results from the Toeplitz determinant (blue dots) for the noninteracting case and the plot of Eq. (95) (dashed line). (b) shows direct numerical results for the interacting case when the Toeplitz determinant is calculated with renormalized parameters found from the mean-field equations (red dots) and the plot of Eq. (98) (dashed line) In both cases, $\mathcal{A} = 1/\pi^{1/8} \approx 0.87$ and $k_F = \pi/6$.

As expected [35], the uniform magnetization in the interacting model has two plateaux, as in Eq. (74). It is shown in Fig. 4. The interaction renormalizes numerical values of critical fields $h_c^{(1,2)}$ and the form of the curve m_z in the IC gapless phase, but not the universal plateau values $m_z = 0, 1$ in two gapped phases. Qualitatively, it means that the interaction does not change the integer-valued filling per unit cell (1 or 0), in agreement with Ref. [36], as one can see in Fig. 9. Thus, the present mean-field theory respects the LSM theorem.

The analytical results of the previous subsection allow us to understand how this interesting feature makes it way through the equations. The renormalized effective spectrum has the same form, as shown in Fig. 8. The bond average

$\mathcal{K}$ and dimerization susceptibility η (cf. (84) and (86)) in the $\mathcal{O}_z(\pi/2)$ phase ($h < h_c^{(2)}$) are h-independent functions of other couplings, see Fig. 2(a). In mathematical terms, these functions form *parabolic lines* of zero curvature in the parametric space. Both quantities $\mathcal{K}$ and η vanish in the PM phase ($h > h_c^{(1)}$). The staggered magnetization m_z^a, cf. (74) and Fig. 4, demonstrates similar behavior. The ground-state energy f in the $\mathcal{O}_z(\pi/2)$ phase is given by the third expression in (71) plus the constant term $\Delta\mathcal{C}$ where $\mathcal{C}$, determined from Eq. (48), is

$$\mathcal{C} = \mathcal{K}^2 + \tfrac{1}{4}\left(m_z^a\right)^2 + \delta^2(\eta^2 + 2\mathcal{K}\eta). \tag{96}$$

The above term and h-independent effective band ε_{eff} lead to f as an h-independent parabolic line at $h < h_c^{(2)}$ [54], and, consequently, $m_z = 0$. For the PM phase with a totally flat band, we find

$$f = -\tfrac{1}{4}\Delta - \tfrac{1}{2}h, \tag{97}$$

where Eq. (42) with $h_R = h - \Delta$ is used, leading to $m_z = 1$ [56]. So, the plateau $m_z = 1$ is due to: (1) flat band which leads to linear dependence of the ground-state energy on the field; (2) the fact that interaction does not renormalize the slope $(-1/2)$ of this straight line. The relation between the magnetization and the winding number (94) holds for the interacting case.

The exact result (92) holds for the plateau of the SOP $\mathcal{O}_z$ in PM phase of the interacting model, along with the step-like h-independent behavior of three parameters $\mathcal{O}_{z,i}$ of the oscillating string long-ranged order, see Figs. 6(a) and 5. Since the interaction does not change the wave vector of the oscillating string order $k_F = \pi/2$, cf. Fig. 9, one can select a convenient single correlation function (63) and to use the SOP $\mathcal{O}_{z,+}$.

It is worth stressing qualitative similarities and distinctions in behaviors of the average quantities entering our equations in two gapped phases: while in the gapped topologically trivial PM phase ($h > h_c^{(1)}$) all quantities m_z, m_z^a, $\mathcal{O}_{z,i}$, $\mathcal{K}$, η are equal to 1 or 0, i.e., they form true plateaux, in the gapped topological phase ($h < h_c^{(2)}$) only the uniform magnetization demonstrates a true (trivial) plateau $m_z = 0$. The other quantities are h-independent functions of other couplings (parabolic lines) [54]. Except for the SOPs, all other quantities are having their values in the gapped phases continuously connected across the IC gapless phase with cusps at two critical points $h_c^{(1)}$ and $h_c^{(2)}$.

The IC gapless phase is the Luttinger liquid (LL) of the JW fermions [8].[2] The long-range string order of the gapped topological phase ($h < h_c^{(2)}$) is taken over by the algebraic order of the power-law decaying string correlations at $h_c^{(2)} < h < h_c^{(1)}$. We have verified numerically oscillating behavior of (57). It is in agreement with predictions (95). In the mean-field approximation, the only effect of interactions on the correlation function is renormalization of k_F and a phase shift. For a comparison with the noninteracting case (95) presented in Fig. 10(a), we chose the model parameters to make the renormalized $k_F = \pi/6$ again. The direct numerical calculations are in excellent agreement with the analytical expression

$$\mathfrak{D}_{zz}(1, n) = \frac{\mathcal{A}}{\sqrt{n+2}} \cos\left(\frac{\pi}{6}(n+2)\right), \tag{98}$$

as one can see from Fig. 10(b). The gapless IC (LL) phase is a counterpart of the floating phase occurring via a BKT thermal phase transition in frustrated 2D Ising models [57,58].

2. *Interaction-driven transition*

The main goals of this subsection is to establish restrictions of the proposed mean-field theory coming from the strength of interactions Δ, and to relate the predicted $\mathcal{O}_z(\pi/2)$-phase to the antiferromagnetic phase known from exact solution. The model of this study is antiferromagnetic, so $\Delta > 0$. Since we are interested to probe effects of the interaction, we turn off other relevant couplings and set $h_a = \delta = 0$.

We analyze the model on the (h, Δ)-plane shown in Fig. 11. As known from exact results [2,4], the chain without external fields generates spontaneous antiferromagnetism (AFM_z) in the axial direction ($m_z^a \neq 0$) at the critical value $\Delta = 1$. At the noninteracting point $\Delta = 0$ the model is in the IC phase at $0 < h < 1$, as we infer from Fig. 1 along the line $\gamma = 0$ [the $\mathcal{O}_z(\pi/2)$ circle is absent, since $\mathcal{R}(h_a = \delta = 0) = 0$]. At $h = 1$ the noninteracting model enters the familiar PM phase. The IC-PM phase boundary $h_c^{(1)} = 1 + \Delta$ is a special case of the exact result (53). At $\Delta > 1$ the AFM_z phase resides inside the V-shaped wedge on the (h, Δ) plane, and at a certain critical field $h = h_c^{(2)}$ the XXZ chain undergoes a phase transition into the IC (LL) phase. This phase boundary, known exactly from the Bethe ansatz, is schematically shown in Fig. 11.

The interaction is a marginal perturbation of the free fermionic Hamiltonian. One can check from the mean-field equations that along with the trivial solution m_z^a, corresponding to the gapless IC state, consistent with the exact results at $\Delta < 1$, those equations admit a nontrivial solution $m_z^a \neq 0$ corresponding to the spontaneously generated antiferromagnetism. The order parameter of this phase is the spontaneous staggered magnetization and it can be found analytically in the regime of weak interaction:

$$m_z^a \approx \frac{2}{\Delta} \exp\left(-\frac{\pi}{2\Delta}\right), \quad \Delta \lesssim 1\,. \tag{99}$$

At large $\Delta \gg 1$, the order parameter saturates towards $m_z^a \sim 1$. A nontrivial m_z^a generates via Eq. (43) the spontaneous staggered field $h_{aR} = \Delta m_z^a$.

We have checked that at the critical value $\Delta = 1$ and $h = 0$, the mean field predicts the ground-state energy of the AFM_z phase $f_{\text{AFM}_z} = -0.4323$, while for the gapless IC phase $f_{\text{IC}} = -0.4196$ with the relative gain of the AFM_z phase about 3%. At $\Delta = 1/2$ and $h = 0$, the parameters are $f_{\text{AFM}_z} = -0.3694$ and $f_{\text{IC}} = -0.3690$, with the relative gain ~0.1%. At smaller Δ the gain is even smaller, and the two states are virtually degenerate. However an unbiased minimization predicts at $h = 0$ the winning antiferromagnetism all the way to $\Delta = 0$,

[2]The mean-field approximation cannot account for such reconstruction of the fermionic ground state due to interactions. Instead of LL, the mean field predicts free fermions, albeit with renormalized parameters. In a moderately minimalist sense, we accept this approximation as adequate, since the exact approach and the mean field both predict a gapless fermionic state.

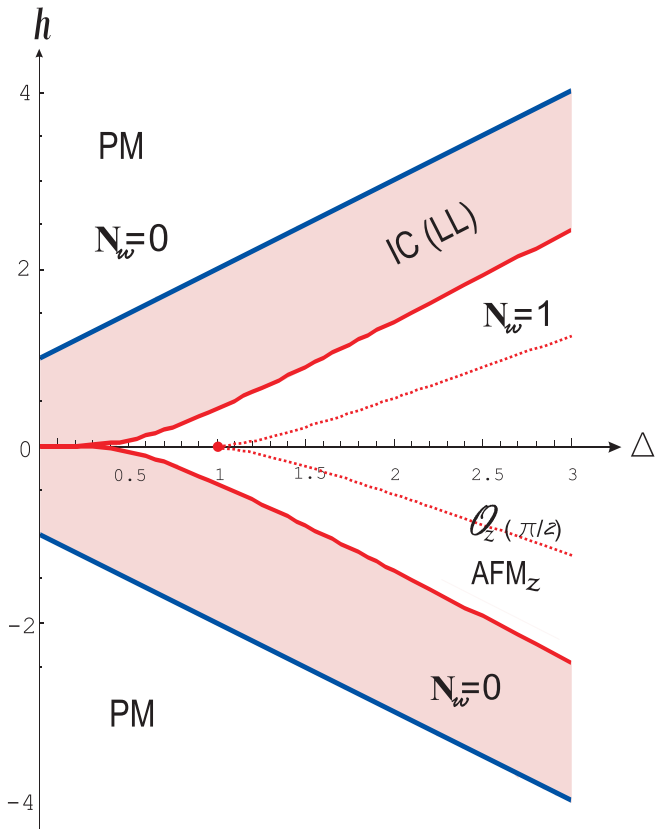

FIG. 11. Phase diagram of the model with zero bare staggered field and dimerization in (h, Δ) plane. The exact result [2,4] for the phase boundary between the phase AFM_z with spontaneous staggered magnetization and gapless IC (LL) phase, ending at the critical point (0,1), is indicated with red dotted line. The bold red line is the mean-field prediction for this boundary. The mean-field approximation agrees with the exact result for the IC-PM phase boundary, shown in bold blue. The topological winding numbers N_w are also shown for each phase.

albeit exponentially weak (99). At $\Delta \lesssim 1$, the mean field predicts the AFM_z-IC phase boundary

$$h_c^{(2)} \sim h_{aR} \approx 2 \exp\left(-\frac{\pi}{2\Delta}\right), \tag{100}$$

while at $\Delta \gg 1$ the critical field $h_c^{(2)}$ crosses over towards

$$h_c^{(2)} \propto \Delta\,. \tag{101}$$

The result of numerical mean-field calculations for $h_c^{(2)}$ is shown in Fig. 11.

The AFM_z-IC phase transition is of the first order in the mean-field theory, since m_z^a undergoes a jump from zero in the gapless IC phase to a finite value and stays constant for a given Δ in AFM_z phase ($h < h_c^{(2)}$). (Note that $\Delta = \text{const}$ lines on the (h, Δ) plane are parabolic lines of h-independent parameters, like f, m_z^a, h_{aR}, etc., as explained above). The spontaneous antiferromagnetism with its primary order parameter m_z^a coexists with the four-periodic string order defined in previous sections. The SOPs are induced by the staggered field $h_{aR} \propto m_z^a$ and are the secondary. The order is of the type (60) with patterns shown in panels (2a) and (2b) in Fig. 7. The string order can be also combined into a single pattern as in Fig. 7 (1) with the help of the correlation function (63). The algebraically ordered gapless IC(LL) phase in Fig. 11 is characterized by the power-law decaying correlation functions, similar to the one shown in Fig. 10.

So the phase with the interaction-induced antiferromagnetism AFM_z on the phase diagram in Fig. 11, *per se* is just a special case of the $\mathcal{O}_z(\pi/2)$ phase shown in Fig. 1. That is why the second label $\mathcal{O}_z(\pi/2)$ for the magneic phase is added in Fig. 11. However, the transition into the gapless IC phase is quite different in two cases, revealing important distinctions between the two phases. The axial symmetry broken in the interaction-generated AFM_z-phase which possesses a sublattice magnetization and doubling of a unit cell, is restored via the first order transition into the IC (LL) phase. The latter, shown in Fig. 11, has both the staggered field and magnetization zero, $m_z^a = h_{aR} = 0$. For the case of the field-generated $\mathcal{O}_z(\pi/2)$-IC transition shown in Fig. 1, *no symmetry breaking related to sublattice (staggered) magnetization occurs, and the field-induced* m_z^a *is not the order parameter.* It is continuous across transition and has a cusp only, as one can see in Fig. 4; the gaplessness of the IC phase is a result of subtle interplay of several relevant couplings. In both cases, of the AFM_z or $\mathcal{O}_z(\pi/2)$ phases, the uniform magnetization m_z is zero, as shown in Fig. 4 ($\gamma = 0$) at $h < h_c^{(2)}$.

The last comment is in order here to address the validity of the proposed mean-field approach. More exactly: how the mean-field prediction of the spurious spontaneous antiferromagnetism with $h_a = \delta = 0$ in the range $\Delta < 1$ can undermine our predictions for the phase diagram in Fig. 1? The answer is twofold: in the absence of relevant terms $\propto h_a$ or $\propto \delta$ and $h = 0$, the mean-field instability in the region $\Delta < 1$ signals the need of that approximation to be replaced by more sophisticated techniques. In the case when one or more of the mentioned parameters are nonzero, the (exponentially weak) interaction-generated terms do not drive spontaneous magnetization, but rather result in innocuous renormalizations of model's parameters. As an example tested by direct simulations, we can mention our earlier work on coupled dimerized XXX chains ($\Delta = 1$) [27,59] where two relevant parameters—dimerization and inter-chain coupling—are present. The mean-field predictions are shown to be very accurate quantitatively, no spurious phases, in agreement with DMRG or exact diagonalization results, even on the lines of quantum criticality where a mutual cancellation of relevant terms occurs.

VI. CONCLUSION

The phase diagram and the order parameters of the XYZ spin-1/2 chain with alternation of the exchange and anisotropy couplings in the presence of uniform and staggered magnetic fields are analyzed. In the fermionic representation, the model is the interacting Kitaev-Majorana chain with hopping, superconducting pairing, and chemical potential modulated. The model is treated within the Landau mean-field framework, where the role of the Ginzburg-Landau potential is played by the effective quadratic fermionic Hamiltonian, derived from the Hartee-Fock (HF) approximation of the interacting fermionic Hamiltonian of the model. The effective HF Hamilonian is expressed in terms of the renormalized

couplings, "dressed" by interactions, which are determined from minimization of the thermodynamic potential. In the noninteracting limit $\Delta = 0$, the HF Hamiltonian recovers the exact one of the free JW fermions, and the renormalized couplings become the bare microscopic parameters of the model.

In this paper, we have worked out all the steps of the framework to deal with an interacting problem involving local and nonlocal orders within the same (extended) Landau formalism. The main progress with respect to the earlier related work [19,25,27], is to present a solution for a physically interesting nonintegrable model, to connect the tools available for the exactly solvable quadratic fermionic Hamiltonians with the standard methods of the mean-field approximation.

The steps of analysis are as follows. Since the effective Hamiltonian is quadratic, its eigenvalues can be found analytically. All possible phases of the model and conditions for the phase boundaries are found from zeros of the spectrum. In case of competing orders, the stable phase is determined by the energy minimum. More physically relevant information is available if analysis of zeros of the spectrum is extended on the complex plane of wave numbers, however it is not always technically straightforward. In this study, such an analysis was done for the axial symmetric limit of the model. On the phase diagram of the model, three possible local order parameters (components of the magnetization) and the nonlocal string order parameter are identified in general case. The local and nonlocal order parameters are expressed via the string correlation functions of Majorana fermions. The latter are evaluated as asymptotes of the determinants of the block Toeplitz matrices. For the effective quadratic Hamiltonian with six renormalized couplings, two unitary matrices of the Bogoliubov transformation were found. These matrices allow to derive an analytic expression for the correlation function of two Majorana fermions, which defines elements of those block Toeplitz matrices. These exact methods are combined with the self-consistent approximation. The latter is a component of the mean-field theory (along with the decoupling and approximation of the Hamiltonian), which uses the minimization of the thermodynamic potential to determine the renormalized couplings (mean-field parameters) of the effective Hamiltonian.

The main result of the above formalism combining the exact and the mean-field methods, is the phase diagram of the model found numerically and shown in Fig. 1, and its local and string order parameters. The representative numerical results for the latter are plotted in Fig. 6. The predictions for conventional (local) orders agree with the earlier results [2,4,7,9,10,42,44] available only for some special choices of parameters of the model we study. We found the topological phase on the diagram with oscillating string order with a period of four lattice spacings which was not reported before for this model. A detailed analysis of patterns of the string order is given. In addition, we have calculated the winding numbers N_w for all phases. The phase with the oscillating topological SOP is the only one with nontrivial $N_w = 1$. In particular, we have shown that the topological winding number cannot change without crossing gapless phase boundary. The present results agree with the recent results for the XY chain [25], which is the noninteraction limit of the current model.

The U(1)-symmetric XXZ limit of the model was given a special consideration. It was demonstrated that the present approach respects the LSM theorem and its implications. In particular, plateaux and h-independent parabolic lines were revealed in various physical quantities, most notable, in the uniform axial magnetization, in accordance with general arguments [35,36,54]. The appearance of the integer-valued and IC fermionic fillings, responsible for qualitatively different behavior of the physical parameters in the gapped and gapless phases, can be qualitatively related to the presence of flat band in the effective single particle spectrum. Turning on the anomalous U(1)-symmetry breaking coupling $\gamma \neq 0$, rounds the flat band and smears plateaux of magnetization and other step-like parameters. The IC (LL) gapless phase with the algebraic order of power-law decaying correlations, is unstable versus any $\gamma \neq 0$, transforming into gapped phases with spontaneous planar magnetization ($m_{x,y}$, depending on the sign of γ). The topological order, which we associate with the oscillating SOP, evolves continuously (albeit not smoothly) through the $\gamma = 0$ line inside the circle on the (h, γ) plane, without gap closing, vanishing order parameter, or changing topological winding number. Similarly, nothing particular happens in the PM phase $h > h_c^{(1)}$ along $\gamma = 0$ line.

So, this line is a gapless line of quantum criticality only at $h_c^{(2)} < h < h_c^{(1)}$ separating gapped AFM phases with planar spontaneous magnetizations $m_{x,y}$. In the topological phase $\mathcal{O}_z(\pi/2)$ inside the circle, the SOP signaling discrete $\mathbb{Z}_2 \otimes \mathbb{Z}_2$ symmetry breaking, demonstrates four lattice spacing periodicity throughout. The line $\gamma = 0$ inside this phase corresponds to additional U(1) symmetry which brings about conserving quantities, but no transition changing the nature of the order in the $\mathcal{O}_z(\pi/2)$ phase, is identified at $\gamma = 0$.

The mean-field results of the present study lay a very good intuitively clear framework for further more technically sophisticated work. Most importantly, direct numerics, like DMRG and/or exact diagonalization, plus heavier analytical guns, like RG and bosonization, are needed to check beyond the mean field the robustness of the predicted phase boundaries and stability of the phases in the sensitive parametric range, along with winding numbers and zero-energy Majorana edge states, with respect to the interaction-driven effects.

ACKNOWLEDGMENTS

We thank F. H. L. Essler and H. Katsura for correspondence. Financial support from the Laurentian University Research Fund (LURF) is gratefully acknowledged.

[1] C. N. Yang and C. P. Yang, Phys. Rev. **147**, 303 (1966); **150**, 321 (1966); **150**, 327 (1966); **151**, 258 (1966).

[2] M. Takahashi, *Thermodynamics of One-Dimensional Solvable Models* (Cambridge University Press, New York, 1999).

[3] B. M. McCoy, *Advanced Statistical Mechanics* (Oxford University Press, New York, 2010).

[4] F. Franchini, *An Introduction to Integrable Techniques for One-Dimensional Quantum Systems*, Lecture Notes in Physics Vol. 940 (Springer, Heidelberg, 2017).

[5] N. Shiraishi, EPL (Europhysics Letters) **128**, 17002 (2019).

[6] E. Lieb, T. Schultz, and D. Mattis, Ann. Phys. **16**, 407 (1961).

[7] M. P. M. den Nijs, Phys. Rev. B **23**, 6111 (1981).

[8] A. Luther and I. Peschel, Phys. Rev. B **12**, 3908 (1975).

[9] F. C. Alcaraz and A. L. Malvezzi, J. Phys. A: Math. Gen. **28**, 1521 (1995).

[10] K. Okamoto and K. Nomura, J. Phys. A: Math. Gen. **29**, 2279 (1996).

[11] J. L. Black and V. J. Emery, Phys. Rev. B **23**, 429 (1981).

[12] B. Bernevig and T. Hughes, *Topological Insulators and Topological Superconductors* (Princeton University Press, Princeton, 2013).

[13] S. Ryu, A. P. Schnyder, A. Furusaki, and A. W. W. Ludwig, New J. Phys. **12**, 065010 (2010).

[14] A. Y. Kitaev, Phys. Usp. **44**, 131 (2001).

[15] J. Alicea, Rep. Prog. Phys. **75**, 076501 (2012).

[16] R. Wakatsuki, M. Ezawa, Y. Tanaka, and N. Nagaosa, Phys. Rev. B **90**, 014505 (2014).

[17] M. Ezawa, Phys. Rev. B **96**, 121105(R) (2017).

[18] J.-J. Miao, H.-K. Jin, F.-C. Zhang, and Y. Zhou, Phys. Rev. Lett. **118**, 267701 (2017).

[19] G. Y. Chitov, Phys. Rev. B **97**, 085131 (2018).

[20] E. Sela, A. Altland, and A. Rosch, Phys. Rev. B **84**, 085114 (2011).

[21] H. Katsura, D. Schuricht, and M. Takahashi, Phys. Rev. B **92**, 115137 (2015).

[22] K. Kawabata, R. Kobayashi, N. Wu, and H. Katsura, Phys. Rev. B **95**, 195140 (2017).

[23] J. Perk, H. Capel, M. Zuilhof, and T. Siskens, Physica A **81**, 319 (1975).

[24] A. Dutta, G. Aeppli, B. K. Chakrabarti, U. Divakaran, T. F. Rosenbaum, and D. Sen, *Quantum Phase Transitions in Transverse Field Spin Models: From Statistical Physics to Quantum Information* (Cambridge University Press, New Delhi, 2015).

[25] G. Y. Chitov, T. Pandey, and P. N. Timonin, Phys. Rev. B **100**, 104428 (2019).

[26] M. den Nijs and K. Rommelse, Phys. Rev. B **40**, 4709 (1989).

[27] G. Y. Chitov and T. Pandey, J. Stat. Mech.: Theory Exp. (2017) 043101.

[28] J. B. Kogut, Rev. Mod. Phys. **51**, 659 (1979).

[29] H.-D. Chen and J. Hu, Phys. Rev. B **76**, 193101 (2007).

[30] X.-Y. Feng, G.-M. Zhang, and T. Xiang, Phys. Rev. Lett. **98**, 087204 (2007).

[31] H.-D. Chen and Z. Nussinov, J. Phys. A: Math. Theor. **41**, 075001 (2008); E. Cobanera, G. Ortiz, and Z. Nussinov, Phys. Rev. B **87**, 041105(R) (2013).

[32] T. Kennedy and H. Tasaki, Phys. Rev. B **45**, 304 (1992); M. Kohmoto and H. Tasaki, *ibid.* **46**, 3486 (1992); M. Oshikawa, J. Phys.: Condens. Matter **4**, 7469 (1992).

[33] K. Nomura, J. Morishige, and T. Isoyama, J. Phys. A: Math. Theor. **48**, 375001 (2015); T. Isoyama and K. Nomura, Prog. Theor. Exp. Phys. **2017**, 103I01 (2017).

[34] F. Pollmann, E. Berg, A. M. Turner, and M. Oshikawa, Phys. Rev. B **85**, 075125 (2012).

[35] M. Oshikawa, M. Yamanaka, and I. Affleck, Phys. Rev. Lett. **78**, 1984 (1997).

[36] M. Oshikawa, Phys. Rev. Lett. **84**, 1535 (2000).

[37] Y. Ogata and H. Tasaki, Commun. Math. Phys. **372**, 951 (2019).

[38] Y. Fei, D. Guo-Hui, and X. Bo-Wei, Commun. Theor. Phys. **37**, 492 (2002); Y. Fei and X. Bo-Wei, *ibid.* **39**, 487 (2003).

[39] J. P. de Lima, L. L. Gonçalves, and T. F. A. Alves, Phys. Rev. B **75**, 214406 (2007).

[40] U. Divakaran, A. Dutta, and D. Sen, Phys. Rev. B **78**, 144301 (2008).

[41] G. Gómez-Santos, Phys. Rev. Lett. **63**, 790 (1989).

[42] D. V. Dmitriev, V. Y. Krivnov, A. A. Ovchinnikov, and A. Langari, J. Exp. Theor. Phys. **95**, 538 (2002); D. V. Dmitriev, V. Y. Krivnov, and A. A. Ovchinnikov, Phys. Rev. B **65**, 172409 (2002).

[43] J.-S. Caux, F. H. L. Essler, and U. Löw, Phys. Rev. B **68**, 134431 (2003); R. Hagemans, J.-S. Caux, and U. Löw, *ibid.* **71**, 014437 (2005).

[44] T. Yamamoto, M. Asano, and C. Ishii, J. Phys. Soc. Jpn. **69**, 3965 (2000).

[45] K. Hida, Phys. Rev. B **45**, 2207 (1992); **46**, 8268 (1992).

[46] Y. Hatsugai and M. Kohmoto, Phys. Rev. B **44**, 11789 (1991).

[47] E. Berg, E. G. Dalla Torre, T. Giamarchi, and E. Altman, Phys. Rev. B **77**, 245119 (2008).

[48] E. Barouch and B. M. McCoy, Phys. Rev. A **3**, 786 (1971).

[49] V. A. Khodel' and V. R. Shaginyan, JETP Lett. **51**, 553 (1990).

[50] G. E. Volovik, J. Exp. Theor. Phys. Lett. **110**, 352 (2019).

[51] V. R. Shaginyan, M. Y. Amusia, A. Z. Msezane, V. A. Stephanovich, G. S. Japaridze, and S. A. Artamonov, J. Exp. Theor. Phys. Lett. **110**, 290 (2019).

[52] A. A. Patel and S. Sachdev, Phys. Rev. Lett. **123**, 066601 (2019).

[53] G. Y. Chitov and C. Gros, Phys. Rev. B **69**, 104423 (2004).

[54] The results for the h-independent quantities in the interacting and noninteracting cases, are in agreement with the results of Watanabe: expectation values of several observables do not depend on magnetic flux in the gapped phases of the model with U(1) symmetry, see H. Watanabe, Phys. Rev. B **98**, 155137 (2018).

[55] Q. Niu, D. J. Thouless, and Y.-S. Wu, Phys. Rev. B **31**, 3372 (1985).

[56] The first exact result on magnetization plateau in the $X\,X\,X$ model with uniform field was reported in R. B. Griffiths, Phys. Rev. **133**, A768 (1964).

[57] J. Villain and P. Bak, J. Phys. France **42**, 657 (1981); P. Bak, Rep. Prog. Phys. **45**, 587 (1982).

[58] G. Y. Chitov and C. Gros, Low Temp. Phys. **31**, 722 (2005); A. Kalz and G. Y. Chitov, Phys. Rev. B **88**, 014415 (2013).

[59] G. Y. Chitov, B. W. Ramakko, and M. Azzouz, Phys. Rev. B **77**, 224433 (2008); S. J. Gibson, R. Meyer, and G. Y. Chitov, *ibid.* **83**, 104423 (2011).